HHS Public Access

Author manuscript

Nature. Author manuscript; available in PMC 2019 April 17.

Published in final edited form as:

Nature. 2018 November ; 563(7729): 113–116. doi:10.1038/s41586-018-0633-x.

A cortico-cerebellar loop for motor planning

Zhenyu Gao[1], **Courtney Davis**[2], **Alyse M. Thomas**[2], **Michael N. Economo**[3], **Amada M. Abrego**[2], **Karel Svoboda**[3], **Chris I. De Zeeuw**[1,4], and **Nuo Li**[2,3]

[1]Department of Neuroscience, Erasmus MC, Rotterdam, the Netherlands [2]Department of Neuroscience, Baylor College of Medicine, Houston TX 77030 [3]Janelia Research Campus, Ashburn VA 20147 [4]Netherlands Institute for Neuroscience, Amsterdam, the Netherlands

Persistent and ramping neural activity in frontal cortex anticipates specific movements [1–6]. Preparatory activity is distributed across multiple brain regions [7,8], but it is unclear which brain areas are involved and how this activity is mediated by multi-regional interactions. The cerebellum is a brain structure thought to be primarily involved in short timescale control of movement [9–12], but roles in cognitive processes have also been proposed [13–16]. In humans, cerebellar damage can cause defects in planning and working memory [13]. We report that persistent representation of information in frontal cortex during motor planning is dependent on the cerebellum. Mice performed a sensory discrimination task in which they used short-term memory to plan a future directional movement. A transient perturbation in the medial deep cerebellar nucleus (fastigial nucleus) disrupted correct subsequent responses, without hampering movement execution. Preparatory activity was observed in both frontal cortex and cerebellar nuclei, seconds before movement onset. Silencing frontal cortex activity abolished preparatory activity in the cerebellar nuclei. Fastigial activity was necessary for maintaining cortical preparatory activity. Fastigial output selectively targeted the behaviorally relevant part of frontal cortex through the thalamus, closing a cortico-cerebellar loop. Our results support the view that persistent neural dynamics during motor planning is maintained by multi-regional neural circuits [17], and that cerebellar computations extend beyond online motor control [13–15,18].

Head-fixed mice discriminated object locations (anterior or posterior) presented during a sample epoch (1.3 s) using their whiskers (Fig. 1a). Mice held their responses in short-term memory and planned for the upcoming movement during a delay epoch (1.3 s). After the

Correspondence: Nuo Li, Baylor College of Medicine, One Baylor Plaza, Houston, TX 77030, nuol@bcm.edu.

Author Contributions

N.L., K.S., C.I.D.Z., and Z.G. conceived the project. Z.G., N.L., and C.I.D.Z. performed pilot experiments. N.L., Z.G., C.D., A.M.T., and A.M.A. performed behavioral and recording experiments. Z.G. performed anatomy experiments. M.N.E. contributed brain alignment software. N.L., Z.G., K.S., and C.I.D.Z. analyzed the data. N.L., Z.G., C.I.D.Z., and K.S. wrote the manuscript with inputs from all authors.

Author information

Reprints and permissions information is available at www.nature.com/reprints. The authors declare no competing financial interests. Readers are welcome to comment on the online version of the paper. Publisher's note: Springer Nature remains neutral with regard to jurisdictional claims in published maps and institutional affiliations. Correspondence and requests for materials should be addressed to N.L. (nuo.li@bcm.edu).

delay epoch, an auditory 'go' cue (0.1s) signaled the response epoch and mice reported pole location by skilled directional licking (left, right) to obtain a water reward.

During the delay epoch, preparatory activity in anterior lateral motor cortex (ALM; Fig 1b) is critical for correct subsequent movements [19–22]. ALM neurons exhibit persistent and ramping activity that predicts specific future movements, long before movement onset.

ALM projects to the cerebellum *via* the basal pontine nucleus [23,24]. We tested cerebellar involvement in the delayed response task by lesioning the fastigial or dentate nucleus (Fig 1c, Methods). We separately examined behavioral choice (the direction of the first lick after the 'go' cue) and movement execution (licking duration and frequency). Fastigial lesions impaired initiation of contralesional licking (Fig 1d) and slowed initiation of contralesional licking following the 'go' cue (Fig 1e). After movement initiation licking was unaffected (Fig 1e, Extended Data Fig 1b–c). Dentate lesions (~1.5 mm away) did not change behavioral choice and movement execution (Fig 1d).

We tested fastigial involvement during specific behavioral epochs by disrupting activity using channelrhodopsin-2 (ChR2) activation (photo-activation, Fig 1f, Methods). Fastigial photo-activation during the early sample epoch had no effect on behavioral choice ($p>0.05$ for either trial type, bootstrap, Methods). Photo-activation during the delay and response epochs both resulted in incorrect choices (Fig 1g–h). Incorrect choices were induced even when the photostimuli ceased 800 ms before the movement. Photo-activation during the delay epoch biased future movements to either the contralateral or ipsilateral direction in individual mice (Fig 1h; Extended Data Fig 1e). Photo-activation immediately before movement onset (response epoch) produced a contralateral bias (Fig 1h), opposite from the directional bias induced by fastigial lesions. Distinct patterns of bias induced by delay versus response epoch photo-activation suggest temporally-specific roles of the fastigial nucleus in driving movement planning versus initiation.

Fastigial photo-activation did not block or perturb the frequency and duration of licking movements after initiation of licking bouts (Fig 1i). Fastigial photo-activation during the delay epoch did not evoke early licks (Extended Data Fig 1f). These data show that rhythmic licking is independent of fastigial activity, but they do not rule out fastigial involvement in controlling the direction and timing of licking bouts *via* its descending input to oscillators in the medulla that drive licking [25]. Dentate photo-activation produced little effect on behavioral choice (Fig 1g, $p=0.06$, bootstrap; Extended Data Fig 1e), consistent with the lesion results.

We tested for necessity by silencing fastigial activity. We photostimulated ChR2 expressing Purkinje cells, which inhibited CN activity (photo-inhibition, Fig 1j; Extended Data Fig 2, Methods). Photo-inhibition during the early sample epoch did not affect behavioral choice (Fig 1k, $p>0.05$ for either trial type, bootstrap, Methods). Photo-inhibition during the late sample and delay epochs resulted in incorrect behavioral choices, with a larger effect induced in the delay epoch (Fig 1k, Extended Data Fig 2g–h). Photo-inhibition during the delay epoch biased future movements to either the contralateral or ipsilateral direction in individual mice (Extended Data Fig 2g–h). Photo-inhibition during movement initiation

(response epoch) produced an ipsilateral bias (Fig 1k), consistent with fastigial lesions, and opposite from the bias induced by fastigial photo-activation. Photo-inhibition minimally affected movement execution (Fig 1l). No other movements were consistently evoked during photo-inhibition (Methods, Extended Data Figs 2e–f, 2i).

Thus, fastigial activity, starting from the late sample epoch and throughout the delay epoch, is required for correct choice.

We compared the activity in ALM and CN by recording from single-units (ALM, n=1194 units; CN, n=564; Extended Data Fig 3; Methods). Most ALM pyramidal neurons distinguished “lick left” and “lick right” trials in spike counts (980/1194, $p<0.05$, two-tailed t-test, Methods). A similar proportion of CN neurons showed trial-type selectivity (416/564). Individual ALM and CN neurons exhibited diverse activity patterns, including selective persistent activity and ramping activity during the delay epoch (Fig 2a–b). Preparatory activity (selectivity before the response epoch) was more prevalent in ALM (ALM, 59% of neurons, CN, 35%; $p<0.001$, chi-square test). Peri-movement activity (selectivity during response epoch) was equally prevalent in both regions (ALM, 67%, CN, 66%). In both regions, a similar proportion (<10%) of neurons modulated their spike rates during individual licks (Extended Data Fig 4).

Selectivity for “lick left” and “lick right” trials emerged gradually in both ALM and CN population averages (Fig 2c–d), starting during the sample epoch and reaching a maximum at the response epoch. On error trials, mice licked in the opposite direction to the instruction provided by object location. A small group of CN neurons signaled object location. However, most CN neurons predicted the upcoming licking direction (67%, Extended Data Fig 4), similar to ALM [19,20]. Thus CN delay epoch selectivity is related to future movement, a hallmark of preparatory activity that instructs subsequent movement.

Preparatory activity was present in all three cerebellar nuclei (Extended Data Fig 3–4). In the fastigial nucleus, distinct patterns of selectivity were observed during the early versus late delay epoch, where equal numbers of neurons preferred either contralateral or ipsilateral movement during the early delay, and a population-level preference for contralateral movement developed right before movement initiation (Extended Data Fig 4g) [23], consistent with the directional biases induced by fastigial lesion and optogenetic manipulations during movement initiation (Fig 1). These results show wide-spread activity related to motor planning and movement initiation in the CN.

The cerebellum is thought to process information over timescales of hundreds of milliseconds [26–28]. Cerebellar preparatory activity lasting over seconds could be inherited from ALM. We recorded from the CN while bilaterally photo-inhibiting ALM during the delay epoch (Fig 3a; Methods). Activity of many CN neurons was rapidly altered by ALM photo-inhibition (185/389, $p<0.01$, two-tailed t-test; latency, 10.7 ± 4.0 ms, mean ± s.e.m.), including neurons with selective persistent and ramping activity (Extended Data Fig 5a). Photo-inhibiting ALM caused a greater proportion of CN neurons to increase their activity, resulting in net disinhibition of CN (Fig 3b, 123/185 increase, 62/185 decrease, $p<0.001$,

binomial test). CN selectivity for “lick left” and “lick right” trials was abolished by photo-inhibiting ALM (Fig 3c, Extended Data Fig 5b–d).

Photo-inhibiting either side of ALM reduced CN preparatory activity (Extended Data Fig 6a–d). Photo-inhibiting motor cortex regions posterior to ALM produced less effect on CN preparatory activity (Extended Data Fig 6e). Thus ALM appears to provide widespread input to the cerebellum to drive CN preparatory activity during motor planning.

We tested whether ALM preparatory activity depends on CN activity by recording from ALM while photo-inhibiting the CN during the delay epoch (Fig 3d; Methods). Activity of many ALM neurons was rapidly altered by CN photo-inhibition (197/454, $p<0.01$, two-tailed t-test, Extended Data Fig 5e; latency, 7.1 ± 3.8 ms). However, the average spike rate was nearly unchanged (control: 4.15 spikes/s; photo-inhibition: 4.39 spikes/s; $p=0.58$, two-tailed t-test). Individual ALM neurons increased (108/197) or decreased (89/197) their responses during CN photo-inhibition (Fig 3e). ALM trial-type selectivity was abolished by CN photo-inhibition (Fig 3f), similar to partial inactivation of the thalamus [17]. Thus, CN activity was necessary for maintaining cortical selectivity for planned movement and preparatory activity is maintained in a cortico-cerebellar loop.

Preparatory activity requires reciprocal excitation between ALM and thalamus [17]. We mapped connectivity between CN, thalamus and ALM using retrograde and anterograde tracers in ALM and CN (Methods, Fig 4a, Extended Data Fig 7–8). Fastigial projections mostly overlapped with parts of the thalamus that project to ALM (i.e., ventral medial nucleus, VM, and parts of anterior-lateral nucleus, VAL), whereas dentate projections targeted an adjacent region that was more dorsal and lateral (i.e., primarily VAL) (Fig 4b–c).

We probed the influence of CN on ALM thalamo-cortical loop during motor planning. We perturbed fastigial or dentate activity using ChR2 activation during the early delay epoch while monitoring ALM preparatory activity (Fig 4d). Fastigial photo-activation induced rapid changes in ALM activity (latency, 4.5 ± 2.6 ms; Extended Data Fig 9a), consistent with a disynaptic pathway through the thalamus. Selective persistent and ramping activity was abolished in most ALM neurons (Fig 4e, top). In a minority of neurons, photo-activation created new preparatory activity (Fig 4e, bottom). Transient photo-activation of the fastigial nucleus altered ALM preparatory activity long (>1 s) after cessation of the photostimulus (Fig 4f; Extended Data Fig 9b). Dentate photo-activation also induced ALM response changes (Fig 4g; latency, 8.3 ± 5.0 ms). Importantly, activity quickly recovered after dentate photo-activation (Fig 4g).

We disambiguated the effect of fastigial and dentate photo-activations on ALM preparatory activity. We analyzed population dynamics in ‘activity space’, where each dimension corresponds to activity of one neuron [6,20,29]. We estimated a ‘coding direction’ (***cd***) in activity space along which preparatory activity maximally discriminated upcoming licking directions (Fig 4h, Methods). In control trials, activity trajectories from “lick left” and “lick right” trials diverged from each other along the ***cd*** during the sample epoch and remained separated throughout the delay epoch, providing a stable neural substrate for a short-term memory of the future movement (Fig 4i) [20]. Fastigial photo-activation resulted in a collapse

of activity trajectories. Additional experiments showed that fastigial photo-activation destroyed the relationship of activity trajectories to specific future movements (Supplementary Information, Extended Data Fig 10). In contrast, dentate photo-activation minimally impacted activity trajectories along the ***cd***, despite having an impact on ALM neuron responses (Fig 4i, Extended Data Fig 9c). Thus fastigial photo-activation destroyed the coding of future movement, whereas dentate photo-activation did not.

Our results show that the cerebellum is critical for the coding of future movement in frontal cortex. Given its roles in movement timing [26], the cerebellum may provide an urgency drive that is necessary for the emergence of selectivity in ALM thalamo-cortical loop [17] in preparation of movement, consistent with attractor models of motor planning [30].

Methods

Mice

This study is based on data from 70 mice (age > P60, both male and female mice, Supplemental Table 1). 13 C57B1/6 mice were used for CN ChR2 photo-activation experiments. A subset of these mice (10 mice) were used for ALM recordings during photo-activation of the CN. Another subset (2 mice) and 6 additional C57B1/6 mice were used for CN lesion experiments (8 mice). 7 L7-cre [31] crossed to Ai32 (Rosa26-LSL-ChR2-EYFP, JAX Stock#012569) [32] mice were used for CN photo-inhibition experiments during behavior. A subset of these mice (4 mice) were used for ALM recordings during CN photo-inhibition. 2 additional L7-cre × Ai32 mice were used to characterize CN photo-inhibition using electrophysiology. 6 additional L7-cre × Ai32 mice (not listed in Supplemental Table 1) were used to quantify general effects of CN photo-inhibition on movements. 10 C57B1/6 mice were used for CN recording experiments. 8 VGAT-ChR2-EYFP mice (Jackson laboratory, JAX Stock#014548) [33] were used for CN recordings during ALM photo-inhibition. 4 VGAT-ChR2-EYFP mice were used for behavioral experiments in which both ALM and CN activity were manipulated to test the causal role of ALM activity in behavior following a fastigial perturbation. 12 C57B1/6 mice (not listed in Supplemental Table 1) were used for anatomical tracing.

All procedures were in accordance with protocols approved by the Institutional Animal Care and Use Committees at Baylor College of Medicine, Janelia Research Campus, and Erasmus Medical Center. Mice were housed in a 12:12 reverse light:dark cycle and tested during the dark phase. On days not tested, mice received 0.5–1 mL of water. On other days, mice were tested in experimental sessions lasting 1 to 2 hours where they received all their water (0.3 to 2 mL). If mice did not maintain a stable body weight, they received supplementary water [34]. All surgical procedures were carried out aseptically under 1–2 % isoflurane anesthesia. Buprenorphine HCl (0.1 mg/kg) or Sustained Release Meloxicam (4mg/kg) was used for pre- and post-operative analgesia. Ketoprofen (5 mg/kg) was used at the time of surgery and post-operatively to reduce inflammation. After the surgery, mice were allowed to recover for at least three days with free access to water before water restriction.

Surgery

Mice were prepared for photostimulation and electrophysiology with a clear-skull cap [19] and a headpost [34]. The scalp and periosteum over the dorsal surface of the skull were removed. A layer of cyanoacrylate adhesive (Krazy glue, Elmer's Products Inc) was directly applied to the intact skull. A custom made headpost was placed on the skull (approximately over visual cortex) and cemented in place with clear dental acrylic (Lang Dental Jet Repair Acrylic; Part# 1223-clear). A thin layer of clear dental acrylic was applied over the cyanoacrylate adhesive covering the entire exposed skull, followed by a thin layer of clear nail polish (Electron Microscopy Sciences, Part# 72180).

In wild-type mice prepared for CN ChR2 photo-activation experiments, 150 nL of AAV2-hSyn1-(h134R)ChR2-EYFP virus (UNC viral core, titer 5.7^{12} vg/ml) was injected in the fastigial nucleus (posterior 2.7 mm from lambda, lateral 0.5 mm, depth 2.3 mm) or dentate nucleus (posterior 2.5 mm lambda, lateral 2.7 mm, depth 2.3 mm), followed by implantation of a 2 mm long optical fiber (Thorlabs, Part#CFML12L02) over the injection site. In VGAT-ChR2-EYFP mice prepared for fastigial perturbation experiments, an optical fiber was implanted at the same stereotaxic coordinate to target the fastigial nucleus.

Behavior

The behavioral task and training have been described [19,34]. The stimulus was a metal pin (0.9 mm in diameter), presented at one of two possible positions (Fig. 1a). The two pole positions were 5 mm apart along the anterior-posterior axis and were constant across sessions. The posterior pole position was 5 mm from the whisker pad. A two-spout lickport (4.5 mm between spouts) was used to deliver water rewards and record answer licks. Behavioral data were acquired using commercial hardware and software (Bpod, Sanworks).

At the beginning of each trial, the vertical pole moved into reach of the whiskers (0.2 s travel time), where it remained for 1 second, after which it was retracted (retraction time 0.2 s). The sample epoch was defined as the time between the pole movement onset to 0.1 s after the pole retraction onset (sample epoch, 1.3 s, Fig. 1a). Mice touched the object at both pole positions, typically with a different set of whiskers. The delay epoch (durations, 1.3 s) followed the sample epoch. An auditory 'go' cue indicated the end of the delay epoch (pure tone, 3.4 kHz, 0.1 s duration). Licking early during the trial was punished by a loud alarm sound (siren buzzer, 0.05 s duration), followed by a brief timeout (1–1.2 s). Licking the correct lickport after the 'go' cue led to a liquid reward (2–3 μL). Licking the incorrect lickport triggered a timeout (2–6 s). Trials in which mice did not lick within a 1.5 second window after the 'go' cue ('no lick') were rare and typically occurred at the end of a session. Reaction time was from the 'go' cue onset to the first lickport contact.

CN Lesion

In 8 wild-type mice, we performed localized lesions in the CN. Intense 473nm light (>10mW) was delivered to either the fastigial or dentate nucleus through the implanted optical fiber for 5–10 min while the mice were under 2 % isoflurane anesthesia. Light-induced heating produced localized lesion around the fiber tip. The lesion areas were estimated *post hoc*, by measuring the size of areas in which neuron labelling were absent

(anti-NeuN staining, Millipore ABN78, 1:1000, Fig 1c, Extended Data Fig 1a). Lesion sizes were between 602–878 um, close to the diameters of the fastigial nucleus or the dentate nucleus. The mice were tested on subsequent days. See Supplemental Table 1 for the list of mice and lesioned hemispheres.

CN ChR2 photo-activation

For ChR2 photo-activation of the CN, 13 wild-type mice injected with AAV2-hSyn1-(h134R)ChR2-EYFP virus were used. Light was delivered to the CN through an optical fiber. In 6 mice, both the fastigial nucleus and the dentate nucleus on opposite hemispheres were tested: left fastigial/right dentate nucleus in 3 mice and right fastigial/left dentate in the other 3 mice. In those mice, the fastigial and dentate nucleus were tested on separate days. In another 3 mice, only the right fastigial nucleus was tested. In another 4 mice, only the right dentate nucleus was tested. In 1 of the fastigial-stimulation mice, the injection of ChR2 virus missed the CN and its data were excluded. See Supplemental Table 1 for the list of mice and manipulated hemispheres in individual experiments.

Light from a 473 nm laser (Laser Quantum, Part# Gem 473) was controlled by an acousto-optical modulator (AOM; Quanta Tech) and a shutter (Vincent Associates). To prevent the mice from distinguishing photostimulation trials from control trials using visual cues, a ‘masking flash’ was delivered using 470 nm LEDs (Luxeon Star) near the eyes of the mice. The masking flash began as the pole started to move and continued through the end of the epoch in which photostimulation could occur. Photostimulation was deployed on 25% of the behavioral trials. During ALM recordings, photostimulation was deployed on 33% of the trials. The photostimulus was pulses of light (5 ms pulse duration) delivered at 20 Hz and a range of peak powers (5, 10, 15mW). The power values reported in the paper indicate average powers (0.5, 1, 1.5 mW). The powers were measured at the fiber tip. The photostimulus started at the beginning of a task epoch and continued for either 0.455 s (10 pulses) or 1.255 s (26 pulses).

We performed photostimulation both during early parts of the sample and delay epochs (0.455 s; Fig 1g–h), as well as the entire epochs (1.255 s; Extended Data Fig 1e). Our primary experiments were centered around sub-epoch manipulations (early sample and early delay). This experimental design was chosen for two reasons. First, sub-epoch manipulations sought to better resolve specific involvements of the CN in time. Manipulations during the entire sample epoch (1.3s) may affect the beginning of motor planning process, and manipulations during the entire delay epoch up to the ‘go’ cue may interfere with movement initiation [20]. Second, we sought to use the early delay epoch manipulation to examine any persistent effect on preparatory activity (Fig 4). If a brain region is involved in maintaining preparatory activity, transiently disrupting it during the early delay should disrupt preparatory activity subsequently. We later tested manipulations that spanned the entire behavioral epochs and included the response epoch to examine the involvement of the CN in movement initiation and execution (Fig 1h–i, Extended Data Fig 1e).

CN photo-inhibition

In L7-cre × Ai32 mice, ChR2 was expressed in cerebellar Purkinje cells. We photostimulated Purkinje cells to inhibit neurons in the CN (Fig 1j). To characterize the effect of CN photo-inhibition (Extended Data Fig 2), we performed silicon probe recordings in the fastigial nucleus (details described in *Electrophysiology*). Photostimulation of Purkinje cells was carried out by directing a blue laser (beam diameter: 400 μm at 4σ) to the brain surface through a cranial window. The photostimulus was a 40 Hz sinusoid (average power, 4.5 mW) lasting for 1.3 sec, including a 100–200ms linear ramp during the laser offset to reduce rebound neuronal activity. Photostimulation was deployed on 25% of the behavioral trials. During ALM recordings, photostimulation was deployed on 33% of the trials. Masking flash was delivered on all trials. Photostimulation was performed at two different locations: 3 mm posterior and 2 mm lateral from lambda (the cerebellar cortex), 1 mm posterior and 2 mm lateral to lambda (the inferior colliculus). Photostimulation of the cerebellar cortex silenced fastigial activity whereas photostimulation of the inferior colliculus did not (Extended Data Fig 2).

For photo-inhibition of the CN during behavior, we tested 7 L7-cre × Ai32 mice. Photostimulation of Purkinje cells was carried out by directing the blue laser to the brain surface through a cranial window. We manipulated the left hemisphere in 3 mice and the right hemisphere in 4 mice. See Supplemental Table 1 for the list of mice and manipulated hemispheres in individual experiments. The photostimulus (average power, 0.5, 1.5, or 4.5 mW) started at the beginning of a task epoch and continued for either 0.5 or 1.3 sec, including the 100–200ms linear ramp.

We performed CN photo-inhibition both during parts of the behavioral epochs (0.5 s; Fig 1k), as well as the entire epochs (1.3 s; Extended Data Fig 2g), for the same reasons described for CN ChR2 photo-activation. In addition to early sample and early delay photo-inhibitions, we also included late sample and late delay photo-inhibitions to resolve CN involvements during specific sub-epochs of the delayed response task (Extended Data Fig 2h). 7 mice were initially tested for sub-epoch photo-inhibitions. Later, 3 of the 7 mice were tested with photo-inhibitions during the entire behavior epochs to confirm the directional bias induced by response epoch photo-inhibition (Extended Data Fig 2g, Supplemental Table 1).

In 4 L7-cre × Ai32 mice (Supplemental Table 1), we recorded from ALM during contralateral CN photo-inhibition. Photo-inhibition (average power, 1.5 or 4.5 mW) started at the beginning of the delay epoch and continued for 1.3 sec, including the 100–200ms linear ramp.

CN photo-inhibition and effects on movement

In 6 naïve L7-cre × Ai32 mice, we examined the general effects of CN photo-inhibition on movements. Two optical fibers were implanted in the fastigial and dentate nucleus on opposite hemispheres to photostimulate Purkinje cell axons in the CN. We tested a range of laser powers (average power, 1.5, 5, 10, 20 mW), including the photostimulus intensities used to photo-inhibit CN activity in the delayed response task (1.5 mW). The photostimulus

was pulses of light (5–10 ms pulse duration, 20–40 Hz, 15–50mW peak powers). Videos (Point Grey, Part# CM3-US-13Y3M-CS or Basler, Part# acA640–300gm) were recorded while mice underwent photo-inhibition either in head-fixed configuration or unrestrained. In head-fixed mice (n=6), jaw movement and eyeblink were tracked using custom software. In unrestrained mice (n=2), the effect of photo-inhibition on movements and postures were manually scored on a scale of 0 to 4 that rated dystonia-like movements [35]: 0 - no motor abnormalities; 1 - slightly slowed or abnormal motor behavior, no dystonia; 2 - mild impairment, mild and transient dystonic postures, weak tremor; 3 - moderate impairment, dystonic postures, cannot balance the body, major tremor; 4 - severe impairment, sustained dystonic postures and limited movements. Two individuals scored the videos independently and the scores were averaged. The scoring was blinded to the experimental conditions.

In head-fixed mice, high-intensity photo-inhibition (20 mW) of the dentate nucleus produced jaw movements (Extended Data Fig 2f). No tongue protrusion was observed in all photo-inhibition conditions. No consistent eyeblink was evoked. At the photo-inhibition intensities used in the delay response task (1.5–5mW), no movement was consistent evoked.

In unrestrained mice, high-intensity photo-inhibition (20 mW) of both the fastigial and dentate nucleus produced dystonia-like movements and posture changes. This included loss of balance and extension of the contralateral limbs (Extended Data Fig 2e). However, at the photo-inhibition intensities used in the delayed response task (1.5–5 mW), no consistent movement was detected (Extended Data Fig 2e).

ALM photo-inhibition

ALM is centered on bregma anterior 2.5 mm, lateral 1.5 mm [19–21]. For photo-inhibition of ALM, we photostimulated cortical GABAergic neurons in VGAT-ChR2-EYFP mice (8 mice). Photostimulation was performed through the clear-skull cap implant by directing the blue laser over the skull (beam diameter: 400 μm at 4σ, bregma anterior 2.5 mm, lateral 1.5 mm). The light transmission through the intact skull was 50% [19]. Photo-inhibition was deployed on 25% of the behavioral trials. During CN recordings, photo-inhibition was deployed on 33% of the trials. Masking flash was delivered on all trials.

We photo-inhibited ALM for 1.3 s at the beginning of the delay epoch, including a 100 ms linear ramp at the laser offset to minimize rebound excitation. This photostimulus was empirically determined to produce robust photo-inhibition in ALM [19,20]. The photo-inhibition silenced 90% of spikes in a cortical area of 1mm radius (at half-max) through all cortical layers. For unilateral ALM photo-inhibition (Extended Data Figs 6, 10), we used a 40 Hz sinusoidal photostimulus (1.5mW average power at the skull surface) at 2.5 mm anterior and 1.5 mm lateral from bregma. For bilateral ALM photo-inhibition (Fig 3, Extended Data Figs 5, 6, 10), we used a constant photostimulus and a scanning galvo (GVSM002, Thorlabs), which stepped the laser beam sequentially through the photo-inhibition sites at the rate of 1 step per 5 ms (step time: 0.2 ms; dwell time: 4.8 ms; measured using a photodiode). 8 photo-inhibition sites were spaced in 1 mm at anterior 2–3 mm and lateral 1–2 mm from bregma, covering ALM. Peak power was adjusted based on the number of photo-inhibition sites to achieve 1.5 mW average power per site.

ALM photo-inhibition after a fastigial perturbation

To test the causal role of ALM activity in driving directional licking after a fastigial perturbation, we tested 4 VGAT-ChR2-EYFP mice (Extended Data Fig 10). We confirmed that ChR2 was expressed in Purkinje cells as well as other GABAergic neurons in the cerebellum [33]. Photostimulation (40 Hz sinusoid; average power, 1.5 mW) was delievered to the fastigial nucleus through an optical fiber to perturb CN activity. Photostimulation started at the onset of the delay epoch and always lasted for 500 ms. We targeted the left fastigial nucleus in 3 mice and the right fastigial nucleus in 1 mouse. See Supplemental Table 1 for the list of mice and manipulated hemispheres. CN perturbations in VGAT-ChR2-EYFP mice might be different from CN photo-activation using ChR2 virus and photo-inhibition in L7-cre × Ai32 mice. We thus first confirmed that in VGAT-ChR2-EYFP mice, fastigial perturbations during the early delay epoch reduced behavioral performance for both trial types (control: “contra lick” trials, 74.5% correct, “ipsi lick” trials, 67.8%; photostimulation: 58.5% and 57.0%; $p<0.05$ for both trial types, bootstrap), similar to other CN optogenetic manipulations during the early delay epoch (c.f. Fig 1h, k).

Photo-inhibition of ALM was performed as described above. For unilateral ALM photo-inhibition, photostimulation started 800 ms after the onset of the delay epoch and ended at the onset of the ‘go’ cue (500ms in duration). Unilateral ALM photo-inhibition before the ‘go’ cue was previously found to bias the upcoming licking to the ipsilateral direction [20]. We confirmed the ipsilateral bias here (Extended Data Fig 6b, 10e). In 3 VGAT-ChR2-EYFP mice, we also tested bilateral ALM photo-inhibition. Bilateral photostimulation started at the onset of the ‘go’ cue and lasted for 1.3 s. On randomly interleaved trials, we either perturbed the fastigial nucleus, or photo-inhibited ALM (unilateral or bilateral), or perturbed the fastigial nucleus followed by ALM photo-inhibition (Extended Data Fig 10f–g). Photostimulation was deployed on 25% of the behavioral trials. Masking flash was delivered on all trials.

Behavioral data analysis

Performance was computed as the fraction of correct choices, excluding lick early trials and no lick trials (Fig 1g, Extended Data Figs 1e, 2g, 10b). Chance performance was 50%. We also separately computed the performance for “lick right” and “lick left” trials (Fig 1; Extended Data Figs 1, 2, 6, 10). Significance of the performance change in each photostimulation condition was determined using bootstrap to account for variability across mice, sessions, and trials. We tested against the null hypothesis that the performance change caused by photostimulation was due to normal behavioral variability. In each round of bootstrap, we replaced the original behavioral dataset with a re-sampled dataset in which we re-sampled with replacement from: 1) mice, 2) sessions performed by each mice, 3) the trials within each session. We then computed the performance change on the re-sampled dataset. Repeating this procedure 10,000 times produced a distribution of performance changes that reflected the behavioral variability. The p-value of the observed performance change was computed as the fraction of times the bootstrap produced an inconsistent performance change (e.g. if a performance decrease was observed during photostimulation, the p-value was the fraction of times a performance increase was observed during bootstrap, one-tailed test).

Electrophysiology

Extracellular spikes were recorded using 32-channel NeuroNexus silicon probes (Part# A4×8–5mm-100–200-177) or 64-channel Cambridge NeuroTech silicon probes (H2 acute probe, 25 μm spacing, 2 shanks). The 32-channel voltage signals were multiplexed, digitized by a PCI6133 board at 400 kHz (National Instruments) at 14 bit, demultiplexed (sampling at 25,000 Hz) and stored for offline analysis. The 64-channel voltage signals were amplified and digitized on an Intan RHD2164 64-Channel Amplifier Board (Intan Technology) at 16 bit, recorded on an Intan RHD2000-Series Amplifier Evaluation System (sampling at 20,000 Hz) using Open-Source RHD2000 Interface Software from Intan Technology (version 1.5.2), and stored for offline analysis.

For ALM recordings, a small craniotomy (diameter, <1 mm) was made one day prior to the recording session (2.5 mm anterior, 1.5 mm lateral from bregma) [19]. A silicon probe was acutely inserted 0.9–1.11 mm below the brain surface prior to the start of each recording session. To minimize brain movement, a drop of silicone gel (3–4680, Dow Corning, Midland, MI) was applied over the craniotomy after the electrode was in the tissue. The tissue was allowed to settle for several minutes before the recording started. 2 to 6 recordings were made from each craniotomy. In 10 mice, recordings were from the left ALM. In 2 mice, recordings were from the right ALM. ALM recordings were always contralateral to the side of CN manipulations (Supplemental Table 1).

For CN recordings, two craniotomies (diameter, 1.5 mm) were made successively over the left cerebellum to target the CN (first at 2.5 mm posterior, 1.5mm lateral from lambda; then at 2 mm posterior, 3 mm lateral from lambda). After a craniotomy was opened, recordings were made at different locations with the craniotomy over the next 5–7 days. A silicon probe was acutely inserted 2.1–2.4 mm below the brain surface prior to the start of each session. On the last recording session, the silicon probe was painted with DiI to label the recording track. All the recording locations within a craniotomy were reconstructed *post-hoc* relative to the labeled track (Extended Data Fig 3). Reconstructions were based on the insertion locations on the brain surface. Recording depths were inferred from manipulator readings and verified based on histology. The second craniotomy was opened after the first craniotomy has been sampled.

Electrophysiology data analysis

The extracellular recording traces were band-pass filtered (300–6 kHz). Events that exceeded an amplitude threshold (4 standard deviations of the background) were subjected to manual spike sorting to extract single-units [19].

For ALM recordings during behavior (Fig 2), 1309 single-units were recorded in 10 mice across 39 sessions. Spike widths were computed as the trough-to-peak interval in the mean spike waveform. Units with spike width < 0.35 ms were defined as fast-spiking neurons (82/1309) and units with spike widths > 0.45 ms as putative pyramidal neurons (1194/1309). Units with intermediate values (0.35 – 0.45 ms, 33/1309) were excluded from analyses. This classification was previously verified by optogenetic tagging of GABAergic neurons [19]. We concentrated our analyses on the putative pyramidal neurons (n=1194). 9 of the 10 mice

were tested with CN ChR2 photo-activation during ALM recordings (Fig 4, Extended Data Fig 10; n=912 putative pyramidal neurons). 1 mouse was excluded because the injection of ChR2 virus missed the CN. For ALM recordings during CN photo-inhibition (Fig 3, Extended Data Fig 5), 490 single-units were recorded in 4 mice across 19 sessions. 454/490 units were putative pyramidal neurons.

For CN recordings during behavior, 878 single-units were recorded in 18 mice across 169 sessions (Fig 2). CN single-units were not classified based on spike shapes. We estimated unit locations based on recording track labeling, recording depth, and the lamination of activity patterns across the recording shanks (Extended Data Fig 3). CN boundaries were visible in DAPI staining (Extended Data Fig 3). 314 units were from outside of the CN (mostly from the cerebellar cortex). 268 units were from the fastigial nucleus, 139 units were from the interposed nucleus, and 157 units were from the dentate nucleus. 8 of the 18 mice were tested with ALM photo-inhibition during CN recordings (Fig 3, Extended Data Figs 5, 6; n=389).

To characterize CN photo-inhibition in L7-cre × Ai32 mice, 60 single-units were recorded in 2 mice across 11 recording sessions (Fig 1j, Extended Data Fig 2). The recordings were targeted to the left fastigial nucleus. 34 units were from outside of CN (mostly from the cerebellar cortex). 26 units were from the fastigial nucleus. The mice were awake but non-behaving during the recordings.

Neurons were tested for significant trial-type selectivity during the sample, delay, or response epochs, using the spike counts from the “lick left” and “lick right” trials (two-tailed *t*-test, $p<0.05$). Neurons that significantly differentiated trial types during any one of the epochs were deemed “selective”. To compute selectivity in Figures 2, 3 and Extended Data Figures 5, 6, we first determined each neuron’s preferred trial type using spike counts from a subset of the trials (10 trials for ALM, 20 for CN), selectivity was calculated as the spike rate difference between “lick left” and “lick right” trials on the remaining data. Selecting preferred trial type using either sample, delay, or response epoch data yielded qualitatively similar preparatory activity.

To quantify the effect of photostimulation on individual neuron spike rates (Figs 3, 4, Extended Data Figs 5, 9), spike counts from “lick left” and “lick right” trials were pooled. We used two-tailed t-tests on spike counts binned in various windows (e.g. Fig 3, and Extended Data Fig 5, the whole delay epoch; Fig 4f, 400 ms time bins in steps of 50ms) to test for significant spike rate change: control versus photostimulation trials.

Quantification of the effect of photostimulation on selectivity was complicated by the fact that selectivity was coupled to upcoming movements (Extended Data Fig 4e). For example, using only correct trials to compute selectivity would miss the trials in which photostimulation caused the mice to switch future movements, thus underestimating the effect of photostimulation on selectivity. We therefore used all trials (correct and incorrect, grouped by instructed trial types) when quantifying selectivity changes caused by photostimulation (Fig 3c, f, Extended Data Figs 5, 6, 9).

Analysis of ALM population dynamics in the activity space

To analyze the relationship between ALM population activity and upcoming movements, we restricted the analysis to the recording sessions with > 5 neurons recorded simultaneously for > 5 trials per condition (28/39 sessions, 8–46 neurons recorded simultaneously; Fig 4, Extended Data Fig 10). For a population of n neurons, we found a $n \times 1$ vector, in the n dimensional activity space that maximally separated the response vectors in “lick right” and “lick left” trials, we term this vector the “coding direction” (***cd***).

Average spike counts were computed in 400 ms windows in 10 ms steps. For each movement direction (“lick right” and “lick left”) we computed the average spike counts $\bar{x}_{lick\,right}$ and $\bar{x}_{lickleft,}$ $n \times 1$ response vectors that described the population response at each time point, t. We computed the difference in the mean response vectors, $cd_t = \bar{x}_{lickrihgt} - \bar{x}_{lickleft}$ $\boldsymbol{cd_t}$ was stable throughout the delay epoch. We averaged the $\boldsymbol{cd_t}$’s from the delay epoch to obtain a single ***cd***. Only correct control trials were used to estimate the ***cd***. The projection along the ***cd*** captured 64.1±3.4% of the population selectivity for “lick left” and “lick right” trials over the sample and delay epochs (root mean square, RMS, of the spike rate difference between “lick right” and “lick left” trials), and 27.0±4.2% of the total variance in ALM task-related activity. Activity variance was quantified as the RMS of the baseline subtracted activity over the sample and delay epochs.

To visualize the effect of CN photo-activation on ALM activity trajectories, we projected the activity trajectories from the control trials, fastigial photo-activation trials, or dentate photo-activation trials on the ***cd***. We used independent control and photo-activation trials from the trials used to compute the ***cd***. For each trial we computed the spike counts for each neuron, ***x*** ($n \times 1$ response vector), at each time point. The projected trajectories in Figure 4i were obtained as $\boldsymbol{cd}^T\boldsymbol{x}$. Both correct and incorrect trials were used to compute the projected trajectries, grouped by the instructed trial types. To average trajectories across multiple behavioral sessions, we first offset the trajectories for a particularly session by subtracting the mean $\boldsymbol{cd}^T\boldsymbol{x}$ across all trials and time points in that session. This removed fluctuations in mean activity from session to session. The offsets were computed using the independent control trials that were used to calculate the ***cd***. Standard errors of the mean was obtained by bootstrapping individual sessions.

To predict upcoming movements using ALM responses projected onto the ***cd*** (Extended Data Fig. 10c–d), we used the response vector ***x*** from the last time bin before the ‘go’ cue (last 400 ms of the delay epoch). For each session, we computed the projected responses, $\boldsymbol{cd}^T\boldsymbol{x}$, from “lick right” and “lick left” trials. The ***cd*** was computed using independent control trials (correct trials only). Separate photostimulation trials were used to predict performance (both correct and incorrect trials). Probability of the mouse licking right in photostimulation trials was calculated as a function of projected responses, $\boldsymbol{cd}^T\boldsymbol{x}$ (Extended Data Fig. 10c–d). Data from multiple sessions were pooled.

Anatomy, tracing

We mapped connectivity between the CN, thalamus, ALM, substantia nigra reticulata (SNr), and the lateral superior colliculus previously implicated to play roles in controlling licking [36]

(Fig 4a–c, Extended Data Figs 7, 8). Mice were anesthetized using isofluorane and fixated on a high precision stereotaxic frame (David Kopf or Stoelting). Coordinates used to target brain areas of interest used either bregma or lambda as the reference points. The coordinates were (in mm): ALM, bregma anterior 2.5, lateral 1.5, depth 0.8; SNr, lambda anterior 1.1, lateral 1.4, depth 4.5; superior colliculus, lambda anterior 0, lateral 1.3, depth 1.8; fastigial nucleus, lambda posterior 2.7, lateral 0.7, depth 2.3; dentate nucleus, lambda posterior 2.5, lateral 2.5, depth 2.4. To label ALM-projecting thalamus, 10% biotin dextran amine BDA-10k (Sigma), or 1% Cholera toxin b subunit Ctb-Alexa647 (Invitrogen) disolved in PBS were iontophoretically injected. Glass pipette with a tip size of 20 um were filled with either BDA or Ctb, 4 mA of positive currents were applied with 7s duty cycle for 15 mins. Viral vector assisted tracing were applied to the other brain regions. 100–150 nl of AAV2-CAG-eGFP or AAV2-CAG-tRFP (UNC viral core, titers 1.0–1.2 × 10^{13} vg/ml) were pressure injected in the target areas. After each injection, the pipette was left in place for >10 minutes before being slowly withdrawn. Brains were processed for immunohistochemistry 10 days after the injection. Mice were deeply anesthetized with an overdose of Nembutal (0.2 ml, i.p.) and transcardially perfused with 20 ml saline followed by 50 ml 4% paraformaldehyde (PFA) in PBS. Brains were extracted and post-fixed in 4% PFA for 2 hours and incubated in 10% sucrose overnight at 4 °C. Brains were then embedded in gelatine and cryoprotected in 30% sucrose in PB, frozen on dry ice, and sectioned using a freezing microtome (50 μm thick). For immunohistochemistry, sections were blocked for 1 hour at room temperature in PBS with 0.4% Triton X-100 and 10% NHS solution and incubation for 48 hrs at 4°C in a mixture of primary antibodies diluted in PBS with 2% NHS and 0.4% Triton X-100. Sections were then washed and incubated for 2 hours at room temperature in the fluorescent secondary antibodies. Axonal projections and neurons were visulized using: mouse anti-NeuN (1:1000, Millipore), chicken anti-GFP (1:2000, Aves), rabbit anti-RFP (1:2000, Rockland), mouse anti-vGlut2 (1:1000, Millipore) and Streptavidin-Alexa647 (1:400, Jackson). Slices were counterstained with DAPI (1:100,000, Invitrogen) and mounted with mounting medium for fluorescence (Mowiol, Sigma). Stacks of images were acquired on an upright LSM 700 confocal microscope (Carl Zeiss, Jena, Germany) operated with Zeiss Zen Software (v2.2) and *post-hoc* adjusted and processed in FIJI software (v.1.46) with appropriate plugins (https://imagej.net/Fiji).

Anatomy, analysis

We aligned each coronal section to the Allen Mouse Common Coordinate Framework (CCF) [37,38] using landmark-based image registration. The registration target was the 10μm/voxel CCF anatomical template. To align a coronal section, we first manually selected the coronal plane in the anatomical template that best corresponded to the section. Next, we manually placed control points at corresponding local landmarks in each image (Extended Data Fig 7a). 30–50 control points were placed in a single image. All control points were outside of the thalamus. Next, the image was warped to the CCF using an affine transformation followed by a nonrigid transformation using b-splines [39]. Images were warped using the B-spline Grid, Image and Point based Registration package available on the Matlab FileExchange (https://www.mathworks.com/matlabcentral/fileexchange/20057-b-spline-grid--image-and-point-based-registration). We performed this procedure independently for

each brain section. 2–6 sections at the rostro-caudal level of the thalamus were analyzed (bregma posterior 1.1–2.1 mm in the CCF).

We quantified the connectivity of the fastigial nucleus, the dentate nucleus, SNr, and superior colliculus with ALM thalamo-cortical loop based on the overlaps in the anterograde fluorescence from a source area with ALM-projecting thalamus. In each case, quantifications of the anterograde fluorescence from a source area were always made in brains that contained co-injections of tracers in ALM to label ALM-projecting thalamus. Injections of retrograde (Ctb) and anterograde (BDA) tracers in ALM produced similar patterns of labeling in the thalamus (Extended Data Fig 8) [17]. We therefore used both types of tracers to label ALM-projecting thalamus. Quantifications of fluorescence were performed on images post alignment to the CCF anatomical template (Extended Data Fig 7b). We found consistent labeling patterns in the thalamus across different injection cases (Extended Data Fig 7c). Alignment to the CCF allowed us to combine quantifications of fluorescence overlaps across different injection cases (Fig 4a–c, Extended Data Fig 7d–f).

To quantify fluorescence overlaps with ALM-projecting thalamus, we first limited the analysis to a subregion of the coronal section that contained the thalamus ipsilateral to the ALM injection (shown in Extended Data Fig 7b at different rostro-caudal levels). We then thresholded the fluorescence intensities independently for each channel at approximately 89^{th} percentile (85^{th}-94^{th} across different cases). The labeled area was defined as all the pixels that exceeded this threshold (Extended Data Fig 7e). Finally, the overlap in fluorescence was computed as the number of pixels co-labeled by ALM injections and a projection (e.g. the fastigial nucleus), divided by the total number of pixels labeled by that projection (“area fraction” overlap, Extended Data Fig 7f). This procedure was carried out separately for each coronal section, which consituted one data point in Fig 4c and Extended Data Figs 7e–f, 8b.

Because we always performed triple injections: a retrograde/anterograde tracer in ALM, and anterograde tracers in two source areas (i.e. the fastigial and dentate nucleus, or the fastigial nucleus and SNr, or the fastigial nucleus and superior colliculus, or other combinations). Quantifications of fluorescence overlaps were further validated by visualizing all three channels in individual injection cases (Extended Data Fig 8).

Statistics

The sample sizes are similar to sample sizes used in the field: for behavior, 3 mice or more per condition; for electrophysiology, more than 100 units per brain region. No statistical methods were used to determine sample size. In 1 of the fastigial photo-activation mice, the injection of ChR2 virus missed the CN and its data were excluded. All key results were replicated in multiple mice. Mice were randomly pre-allocated into experimental groups. Unless stated otherwise, the investigators were not blinded to allocation during experiments and outcome assessment. Trial types were randomly determined by a computer program. During spike sorting, experimenters cannot tell the trial type, so experimenters were blind to conditions. Statistical comparisons using t-tests and bootstrap are described in detail in sections above.

Code availability

Software used for data analysis is available from the corresponding author upon reasonable request.

Data availability

Raw and processed data are available from the corresponding author upon reasonable request.

Extended Data

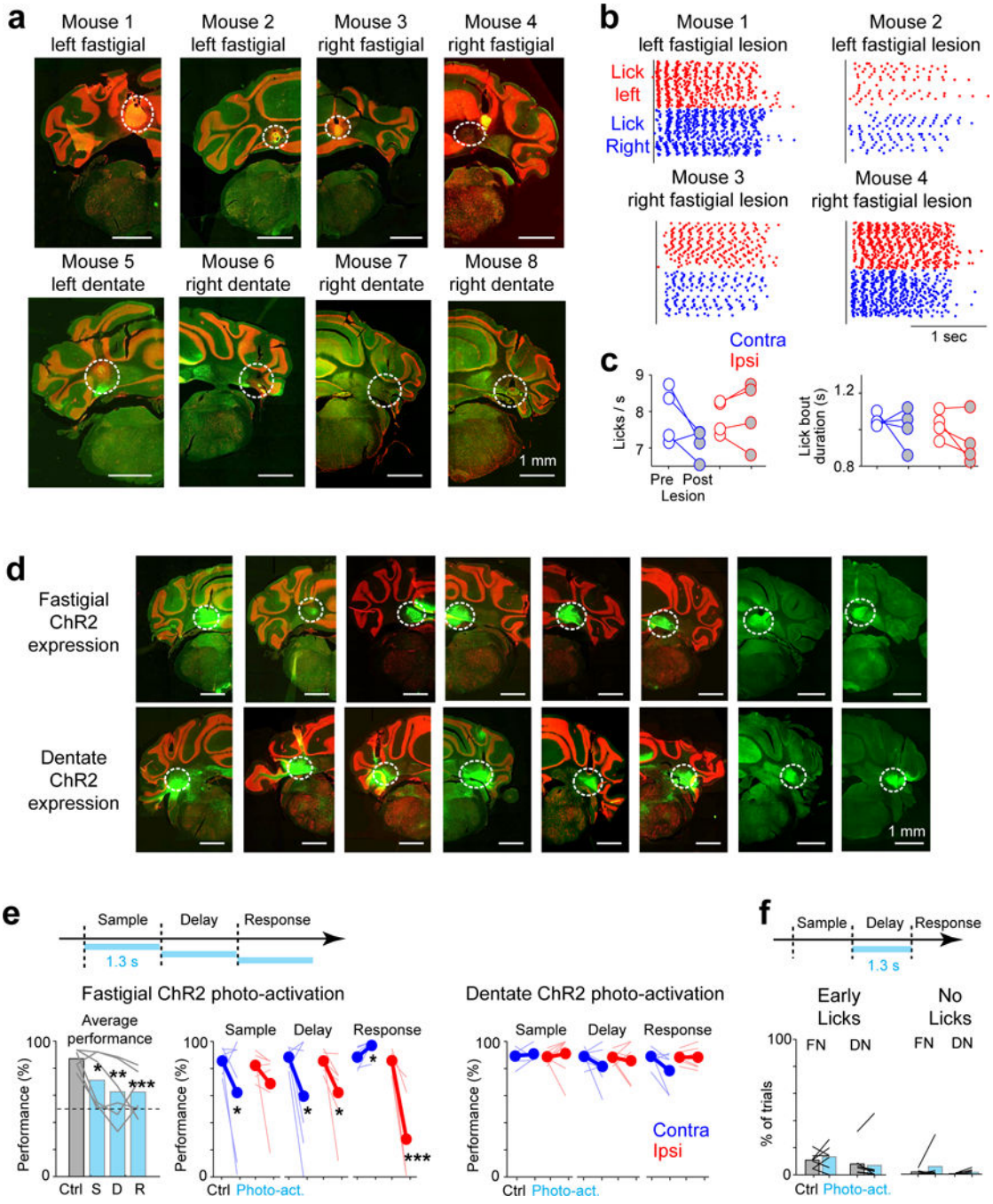

Extended Data Figure 1. Histology and behavioral data.

a. Coronal sections showing CN lesion sites for all mice. Fastigial lesion, n=4; dentate lesion, n=4.

b. Licking movement is not affected by fastigial lesion. Individual licks are shown as dots (blue, lick right; red, lick left). Licks are aligned to the onset of the ‘go’ cue (vertical line).

c. Average lick rate within a lick bout and the duration of lick bouts are not affected by fastigial lesion. A lick bout is defined as a sequence of licks with inter-lick-interval less than 500 ms. Data from the fastigial-lesion mice only (n=4). Data are grouped by licking direction relative to the lesioned hemisphere: contralesional licking (blue) or ipsilesional licking (red).

d. Coronal sections showing ChR2-EYFP expression in the fastigial and dentate nucleus. 9 mice were used for various fastigial ChR2 photo-activation experiments, and 10 mice were used for dentate ChR2 photo-activation experiments. In 1 of the fastigial photo-activation mice, the injection of ChR2 virus missed the CN (not shown) and its data were excluded. 2 of the dentate photo-activation mice were subsequently used for lesion experiments (not shown). See Supplemental Table 1 for the list of mice and manipulated hemispheres in individual experiments.

e. CN photo-activation during specific behavioral epochs. *Top*, experiment timeline. Photostimulation was for the entire task epoch (1.3 s). *Bottom*, behavioral performance. *Left*, fastigial photo-activation (n=6); *right*, dentate photo-activation (n=8). For fastigial photo-activation, average behavioral performance for control and photo-activation trials (S, sample epoch photo-activation; D, delay epoch; R, response epoch) is also shown. Gray lines show individual mice. Chance is 50%. For behavioral performance grouped by trial type, “lick left” and “lick right” trials are grouped by instructed licking direction relative to the manipulated hemisphere. Blue, contralateral; red, ipsilateral. Both hemispheres were tested. See Supplemental Table 1 for the list of mice and manipulated hemispheres. Thick lines, mean; thin lines, individual mice (n=6). *, $p<0.05$, **, $p<0.01$, ***, $p<0.001$, one-sided test, bootstrap (Methods).

f. Early lick rate and no lick rate with and without CN photo-activation during the delay epoch. Control trials (gray) and photo-activation trials (cyan). Lines, individual mice. FN, fastigial photo-activation (n=6); DN, dentate photo-activation (n=8).

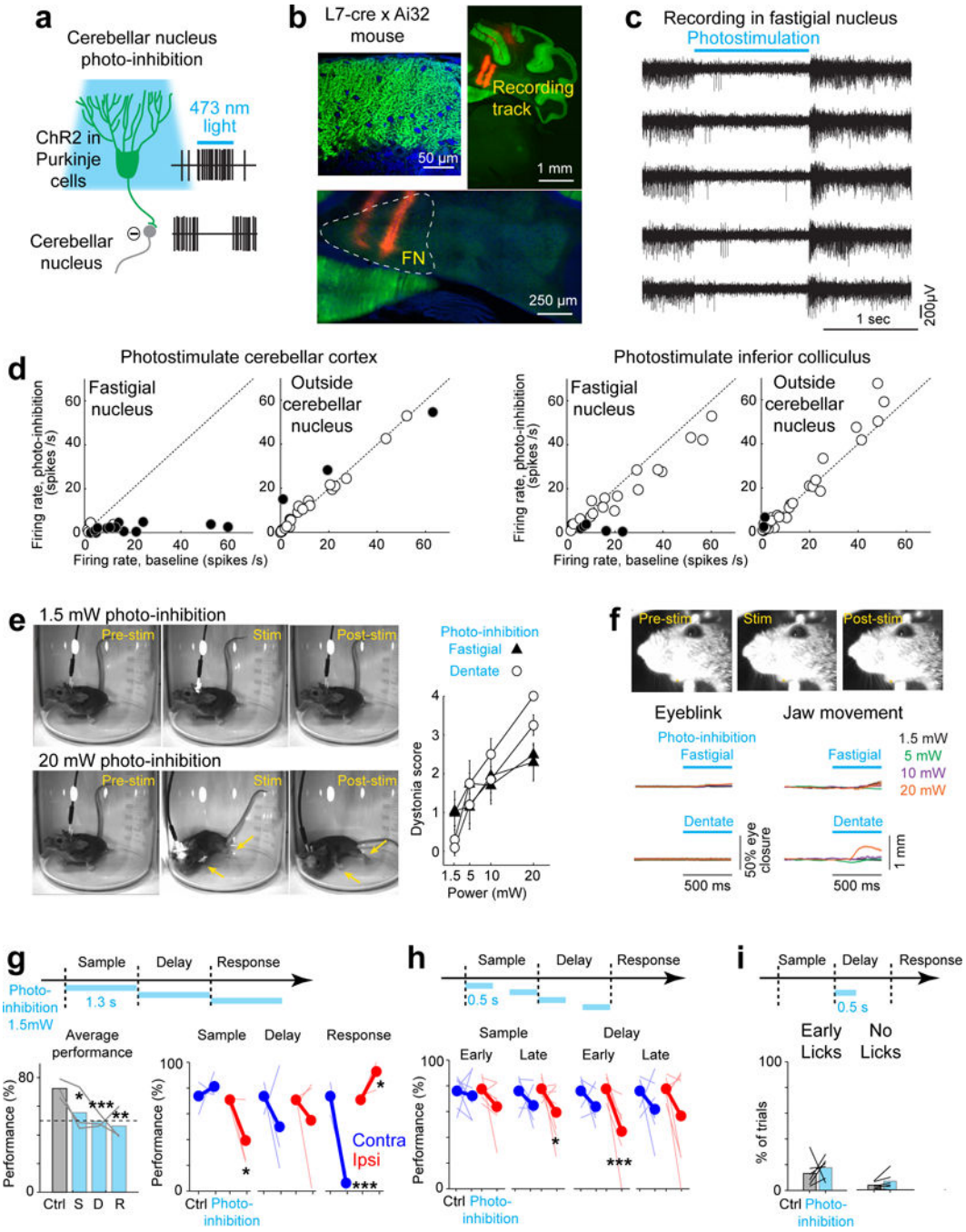

Extended Data Figure 2. Characterization of CN photo-inhibition and behavioral data.

a. Strategy to silence the CN. *Left*, ChR2 is expressed in cerebellar Purkinje cells. Photostimulation of Purkinje cells inhibits CN neurons (‘photo-inhibition’).

b. *Top left*, an image of the cerebellar cortex showing ChR2-EYFP expression in Purkinje cells in L7-cre × Ai32 mouse. *Top right*, an example silicon probe recording in a L7-cre × Ai32 mouse. The coronal section shows ChR2-EYFP expression in the cerebellar cortex and DiI labeled electrode tracks. *Bottom*, electrode tracks within the fastigial nucleus (dashed contour). Photostimulation of Purkinje cells was carried out by directing a blue laser (0.5–

4.5 mW average power, beam diameter: 400 μm at 4σ) to the brain surface through a cranial window.

c. Example voltage traces from a fastigial nucleus recording during photo-inhibition. Multi-unit activity in the fastigial nucleus was silenced. Multiple traces show repeats of photostimulation.

d. Photo-inhibition reduced activity specifically in the CN. Average spike rates before (500 ms) versus during photo-inhibition (1.2 s). Neurons from the fastigial nucleus (*left*, n=26) and from the surrounding cerebellar cortex (*right*, n=34). Photostimulation of the cerebellar cortex (lambda posterior 3 mm, lateral 2 mm) silenced fastigial activity whereas photostimulation of the inferior colliculus (posterior 1mm, lateral 2mm) did not. Solid dots, neurons with significant spike rate change ($p<0.01$, two-tailed t-test).

e. Dose dependent effect of CN photo-inhibition on posture and movement. *Left*, video frames showing an unrestrained mouse undergoing CN photo-inhibition. During low-intensity photo-inhibition (1.5mW, the intensity typically used in the delayed response task), no consistent movement was detected. High-intensity photo-inhibition (20 mW) of both the fastigial and dentate nucleus produced dystonia-like movements and posture changes, such as loss of balance and extensions of the contralateral limbs (arrows). *Right*, scores that rated dystonia-like movements on a scale of 0–4 (Methods): 0 - no motor abnormalities; 1 - slightly slowed or abnormal motor behavior, no dystonia; 2 - mild impairment, mild and transient dystonic postures, weak tremor; 3 - moderate impairment, dystonic postures, cannot balance the body, major tremor; 4 - severe impairment, sustained dystonic postures and limited movements. The scoring was blinded to the experimental conditions. Mean ± s.e.m. across trials. N=2 mice, 10 trials per condition.

f. Dose dependent effect of CN photo-inhibition on jaw movement and eyeblink. *Top*, video frames showing a head-fixed mouse undergoing CN photo-inhibition. *Bottom left*, eyeblink responses during CN photo-inhibition. No consistent eyeblink was evoked. *Bottom right*, jaw movements during CN photo-inhibition. Only high-intensity photo-inhibition (20 mW) of the dentate nucleus produced jaw movements. Mean ± s.e.m. across trials. N=4 mice, 10 trials per condition for eyeblink, 20 trials per condition for jaw movement.

g. Behavioral performance in the delayed response task with and without fastigial photo-inhibition. Photo-inhibition during the entire task epochs (n=3). *Left*, average behavioral performance for control and photo-inhibition trials (S, sample epoch photo-inhibition; D, delay epoch; R, response epoch). Gray lines show individual mice. Chance is 50%. *Right*, behavioral performance for each trial type. “Lick left” and “lick right” trials are grouped by instructed licking direction relative to the manipulated hemisphere. Blue, contralateral; red, ipsilateral. Both hemispheres were tested. See Supplemental Table 1 for the list of mice and manipulated hemispheres. Thick lines, mean; thin lines, individual mice. *, $p<0.05$, **, $p<0.01$, ***, $p<0.001$, one-sided test, bootstrap (Methods).

h. Behavioral performance. Photo-inhibition during the early sample, late sample, early delay, and late delay epochs (n=7 mice). *, $p=0.04$, ***, $p=0.0002$, one-sided test, bootstrap.

i. Early lick rate and no lick rate during delay epoch fastigial photo-inhibition. Control trials (gray) and photo-inhibition trials (cyan). Lines, individual mice (n=7).

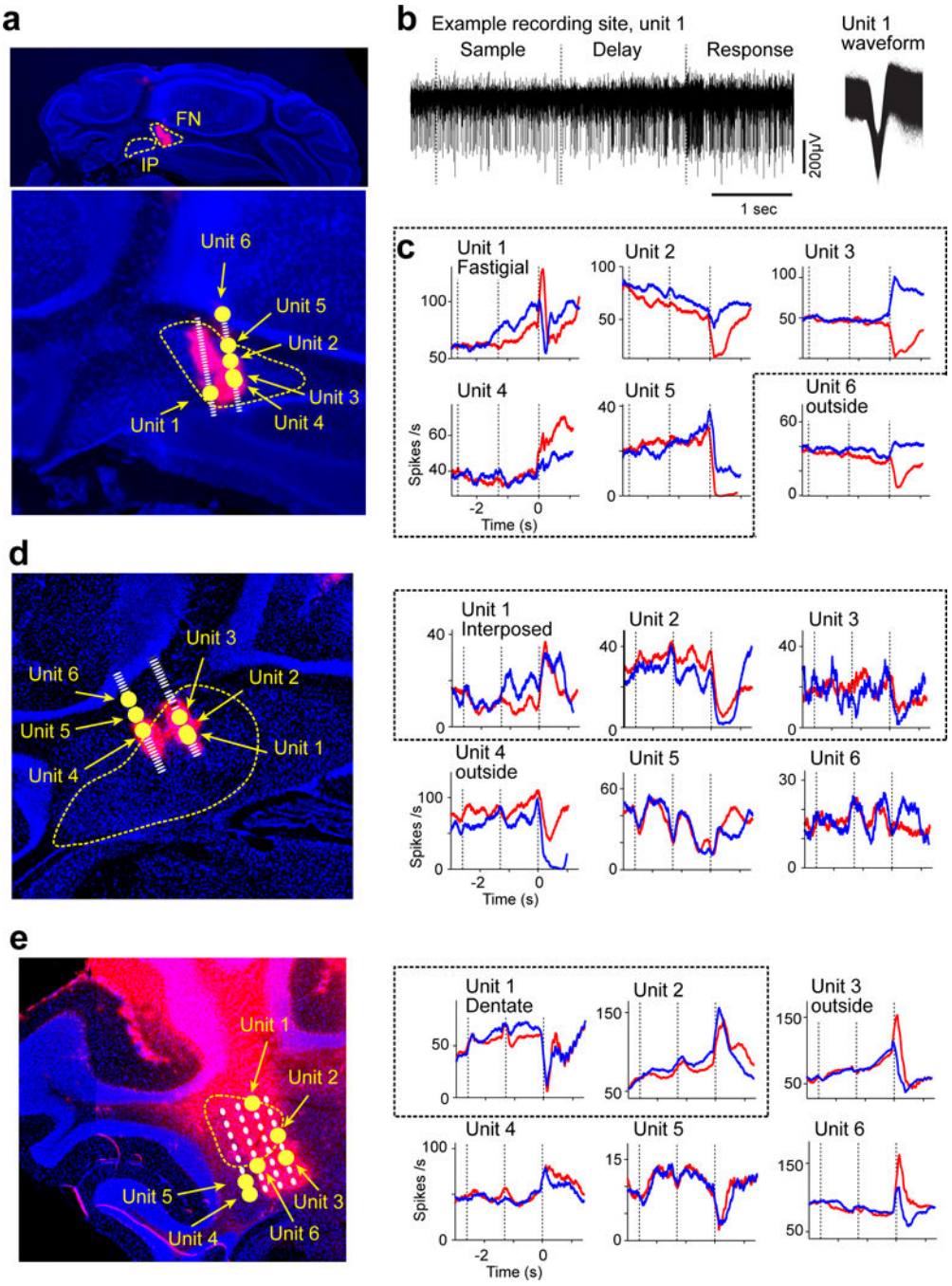

Extended Data Figure 3. Silicon probe recordings in the CN.

a. DiI labeled recording tracks in coronal sections stained by DAPI. Borders of the CN were visible in DAPI staining. Electrode location was estimated based on DiI labeling and manipulator depth. The lamination of activity patterns across the electrodes corresponded well to the anatomical structures: i.e. high activity level in the CN and cerebellar cortex, low activity level in the white matter. Single-unit locations were estimated based on electrode location. *Top*, a coronal section showing a recording in the fastigial nucleus. *Bottom*, the

fastigial nucleus (yellow dashed line), estimated electrode location, and the locations of single-units (units 1–6) from an example recording.

b. *Left*, voltage trace from the recording site of unit 1 during a single behavioral trial. Dashed lines, behavioral epochs. *Right*, waveforms of unit 1 after spike sorting.

c. PSTHs of all the units from the example fastigial recording. Dashed box indicates that units 1–5 were within the fastigial nucleus. Unit 6 was outside of the fastigial nucleus. Blue, "lick right" trials; red, "lick left" trials.

d. Same as **a** and **c**, but for an example recording in the interposed nucleus.

e. Same as **a** and **c**, but for an example recording in the dentate nucleus.

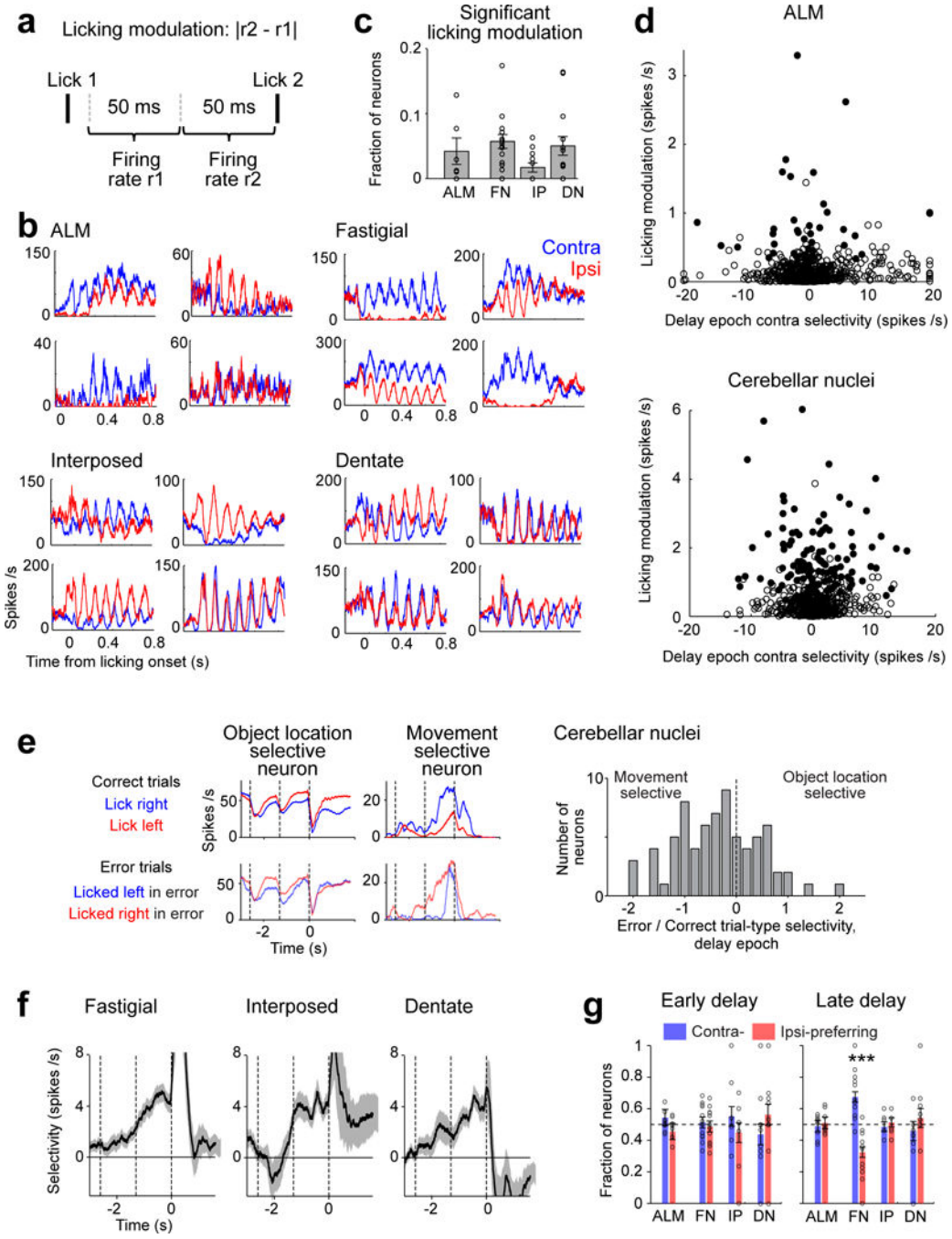

Extended Data Figure 4. ALM and CN activity related to motor planning and movement.

a. Criteria used to identify neuronal activity modulated by licking. For each lick, spike counts were calculated in two adjacent 50ms time windows, starting 20ms from the detection time of the lick. Across all licks and all trials, neurons with significant spike count difference between the two time windows were deemed to be modulated by licking ($p<0.01$, two-tailed t-test). Licking modulation is calculated for each neuron: mean spike rate difference between the two time windows.

b. Example neurons significantly modulated by licking. PSTH from the correct “lick right” and “lick left” trials during the response epoch. Spike times are aligned to the first lick. Trials are grouped by licking direction relative to the recorded hemisphere: contralateral (blue) or ipsilateral (red). Averaging window, 10 ms.

c. Fraction of neurons significantly modulated by licking ($p<0.01$, two-tailed t-test) from each brain region. ALM, the anterior lateral motor cortex; FN, the fastigial nucleus; IP, the interposed nucleus; DN, the dentate nucleus. Error bars, s.e.m. across mice, bootstrap (Methods). Dots, individual mice (ALM, n=10; FN, n=15; IP, n=9; DN, n=11).

d. No correlation between whether a neuron was modulated by licking and whether it exhibited preparatory activity. *Top*, ALM; *bottom*, the cerebellar nuclei. Selectivity during the delay epoch is the spike rate difference between the “lick right” and “lick left” trials. Solid dots, neurons with significant licking modulation ($p<0.01$, two-tailed t-test).

e. Preparatory activity in the CN. *Left*, 2 example CN neurons. PSTHs for correct and error trials. Trial types are based on sensory instruction (blue, “lick right”; red, “lick left”). The same trial-type preference in correct and error trials indicates selectivity for object location. Opposite trial-type preference indicates selectivity for upcoming movement directions. A negative ratio of trial-type selectivity between error and correct trials means a neuron switches trial-type preference to predict upcoming movement directions on error trials. *Right*, selectivity ratios for CN neurons. Neurons with significant delay epoch selectivity and tested for >3 error trials (n=73).

f. Population selectivity for each cerebellar nucleus (mean ± s.e.m. across neurons, bootstrap; fastigial, n=87; interposed, n=50; dentate, n=60). Selectivity is the spike rate difference between the preferred and non-preferred trial type (Methods). Dashed lines separate sample, delay and response epochs.

g. Proportion of contra- versus ipsi-preferring neurons based on spike counts during the first 500ms (*left*) and the last 500ms (*right*) of the delay epoch. Error bars, s.e.m. across mice. Dots, individual mice (ALM, n=10; FN, n=15; IP, n=9; DN, n=11). ***, p=0.0001, one-sided test, bootstrap.

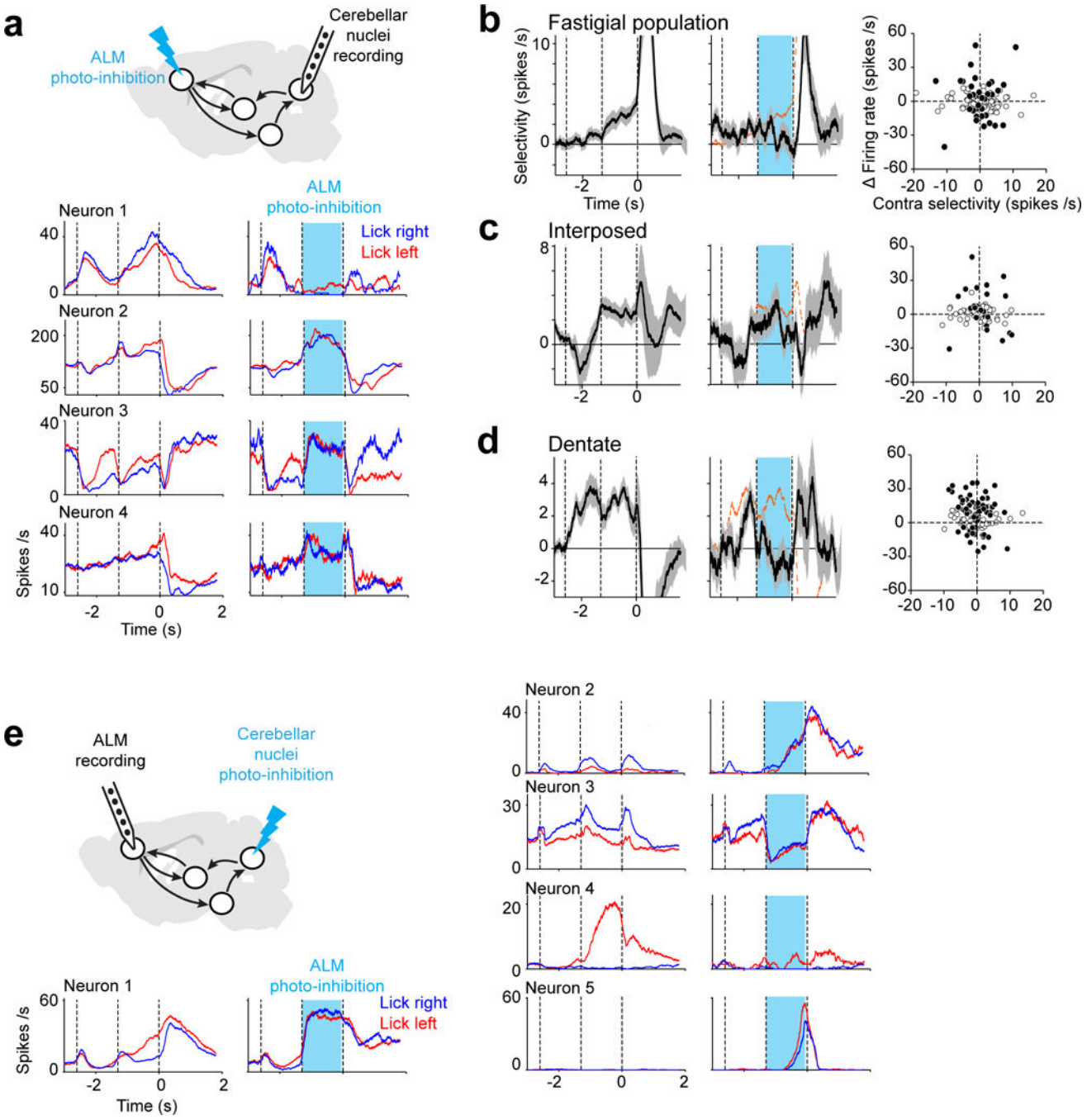

Extended Data Figure 5. ALM drives CN preparatory activity and *vice versa*.

a. *Top*, schematic showing CN recording during bilateral ALM photo-inhibition. Laser power, 1.5 mW per location (Methods). *Bottom*, PSTHs of 4 example CN neurons with and without ALM photo-inhibition. Cyan, photo-inhibition. Blue, “lick right” trials; red, “lick left”.

b. *Left*, average fastigial selectivity in control and photo-inhibition trials (mean ± s.e.m. across neurons, bootstrap). Only selective neurons tested for >3 trials in all conditions are included (n=54 neurons, 8 mice). Orange dashed line, mean from control trials. *Right*,

relationship between delay epoch selectivity of individual fastigial neurons and changes in firing rate due to ALM photo-inhibition. Filled circles, neurons significantly modulated by ALM photo-inhibition ($p<0.01$, two-tailed t-test).

c. Same as **b**, but for the interposed nucleus (n=44 neurons, 5 mice).

d. Same as **b**, but for the dentate nucleus (n=59 neurons, 6 mice).

e. Same as **a**, but for ALM recording during contralateral CN photo-inhibition. Laser power, 1.5–4.5 mW.

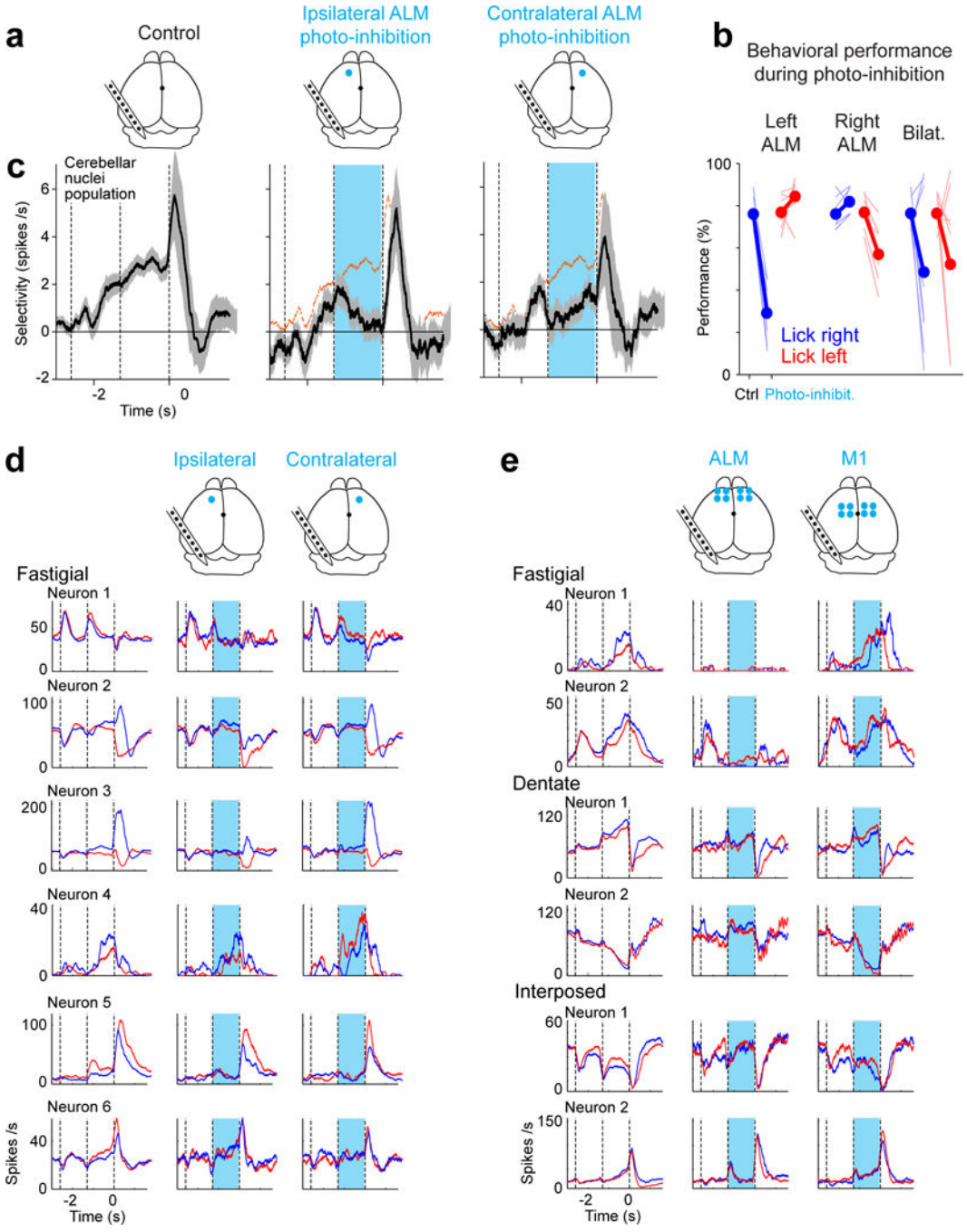

Extended Data Figure 6. CN preparatory activity is driven by both hemispheres of ALM.

a. CN recording during contralateral or ipsilateral ALM photo-inhibition.

b. Behavioral performance during unilateral and bilateral ALM photo-inhibition.

c. CN population selectivity from control and photo-inhibition trials (mean ± s.e.m. across neurons, bootstrap). Only selective neurons tested for >3 trials in all conditions are included (n=157). Orange dashed line, mean from control trials. Cyan, photo-inhibition. CN selectivity was reduced by photo-inhibiting either side of ALM.

d. Example CN neurons during ipsilateral or contralateral ALM photo-inhibition. The effect was heterogeneous across individual neurons. Some neurons were affected by ipsilateral ALM photo-inhibition (row 1–3), other neurons were affected by contralateral ALM photo-inhibition (row 4), others were affected by photo-inhibiting either side (row 5, 6).

e. Example CN neurons during bilateral ALM or M1 photo-inhibition. ALM, bregma anterior 2–3 mm, lateral 1–2 mm; M1 anterior 0–1 mm, lateral 1–2 mm.

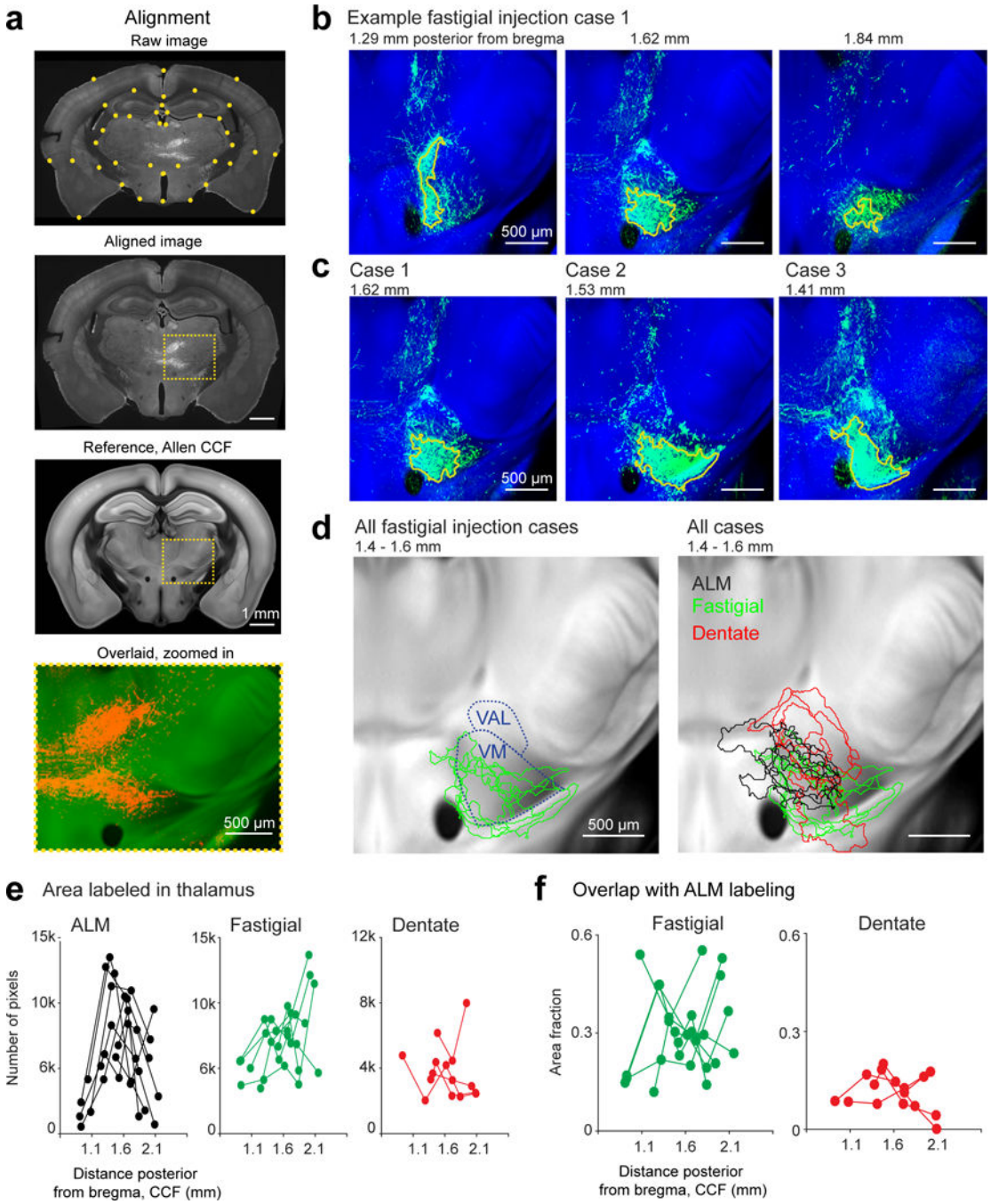

Extended Data Figure 7. Alignment of anatomical data and comparing fastigial and dentate projections to ALM-projecting thalamus.

a. *Top*, an example coronal section before and after alignment to the corresponding section of the anatomical template in the Allen Mouse Common Coordinate Framework (CCF). Fluorescence is anterograde labeling (BDA) from an ALM injection, labeling the ALM-projecting thalamus (Methods). Yellow dots, control points for b-spline transformation. Dashed line, a region of interest containing the thalamus ipsilateral to the ALM injection. *Bottom*, overlay of the aligned image (red) and the anatomical template (green). ALM axons

in the thalamus obey structural boundaries in the anatomical template. Critically, the alignment procedure did not use any structures inside the thalamus as landmarks.

b. Coronal sections showing an example fastigial injection case with anterograde labeling in the thalamus. The sections are aligned to and superimposed on the anatomical template. The yellow outlines show labeled areas after thresholding (Methods).

c. Coronal sections showing 3 different fastigial injection cases. Different injections show similar patterns of anterograde labeling in the thalamus.

d. *Left*, outlines of the labeled areas from all fastigial injection cases (n=6). Borders of the thalamic nuclei (VM and VAL) are based on annotations in the Allen Reference Brain. *Right*, outlines of the labeled areas from all fastigial (n=6), dentate (n=4), and ALM (n=8) injection cases. There was a greater overlap between fastigial and ALM labeling.

e. Total areas labeled (number of pixels) in the thalamus by fastigial, dentate, and ALM injections. Dots, individual coronal sections. Lines, individual injections.

f. Overlaps between fastigial/dentate projections and ALM-projecting thalamus. The co-labeled area is normalized to the total thalamic area labeled by fastigial/dentate projections (‘area fraction overlap’). Dots, individual coronal sections. Lines, individual injections.

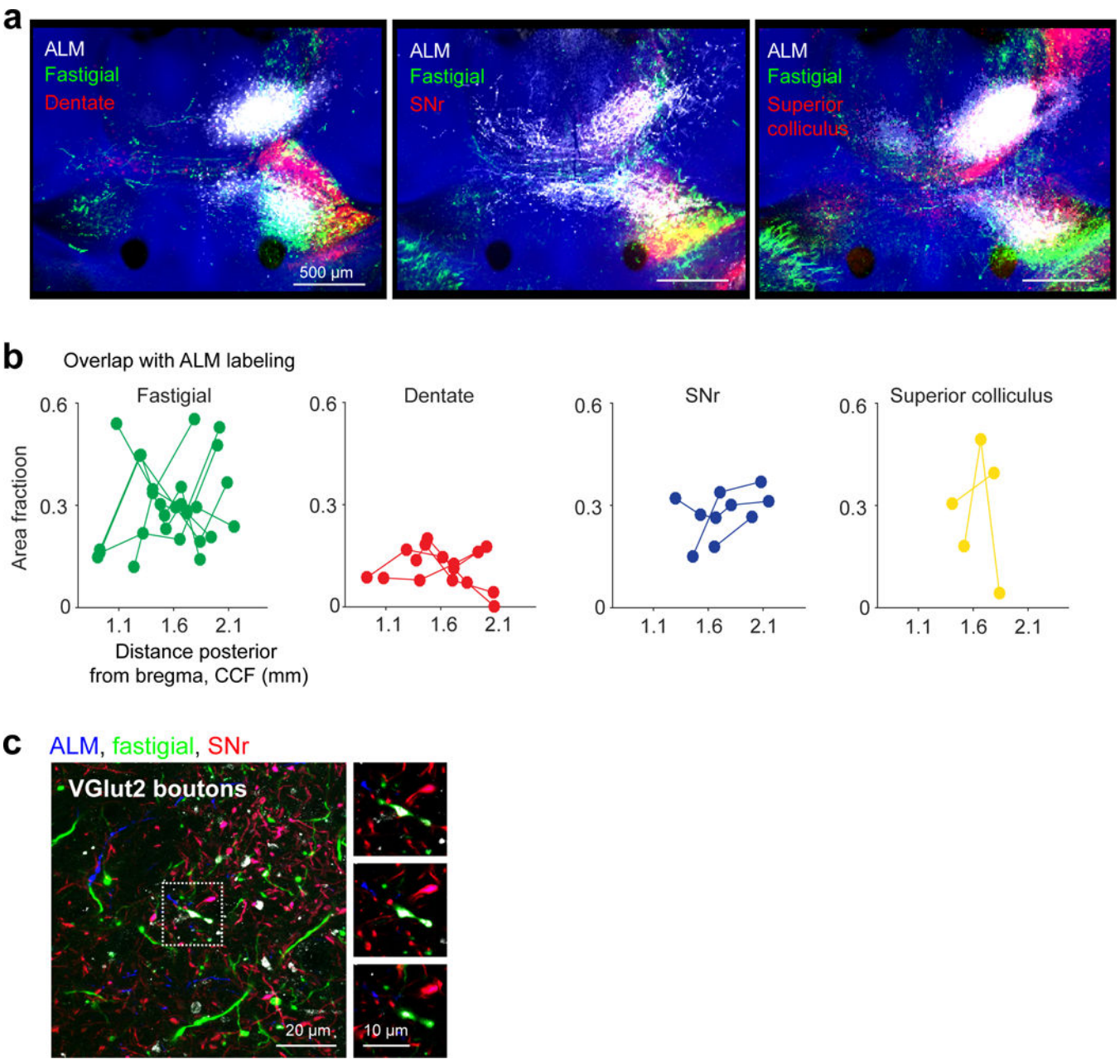

Extended Data Figure 8. ALM-projecting thalamus receives converging inputs from the fastigial nucleus, basal ganglia substantia nigra reticulata (SNr), and superior colliculus.

a. Example triple injections showing co-labeling of fastigial and dentate projections (*left*), fastigial and SNr projections (*middle*), and fastigial and superior colliculus projections (*right*) in the thalamus. Injections were repeated multiple times in different mice with similar results (ALM-fastigial-dentate, n=4; ALM-fastigial-SNr, n=3; ALM-fastigial-superior colliculus, n=2).

b. Overlaps between ALM-projecting thalamus and projections of different areas (Methods). Fastigial, SNr, and superior colliculus labeling show comparable amount of overlaps with ALM-projecting thalamus. Dentate labeling show less overlap. The thalamic area co-labeled by ALM injection and a projection (fastigial, dentate, SNr, or superior colliculus) is

normalized to the total thalamic area labeled by that projection (‘area fraction’). Dots, individual coronal sections. Lines, individual injections.

c. A confocal image showing vGlut2 staining in ALM-projecting thalamus. Anterograde tracer injections in ALM (blue), the fastigial nucleus (green), and SNr (red). Fastigial axons form glutamatergic synapses (vGlut2 positive) within ALM-projecting thalamus. vGlut2 staining was performed in one ALM-fastigial-SNr injection case.

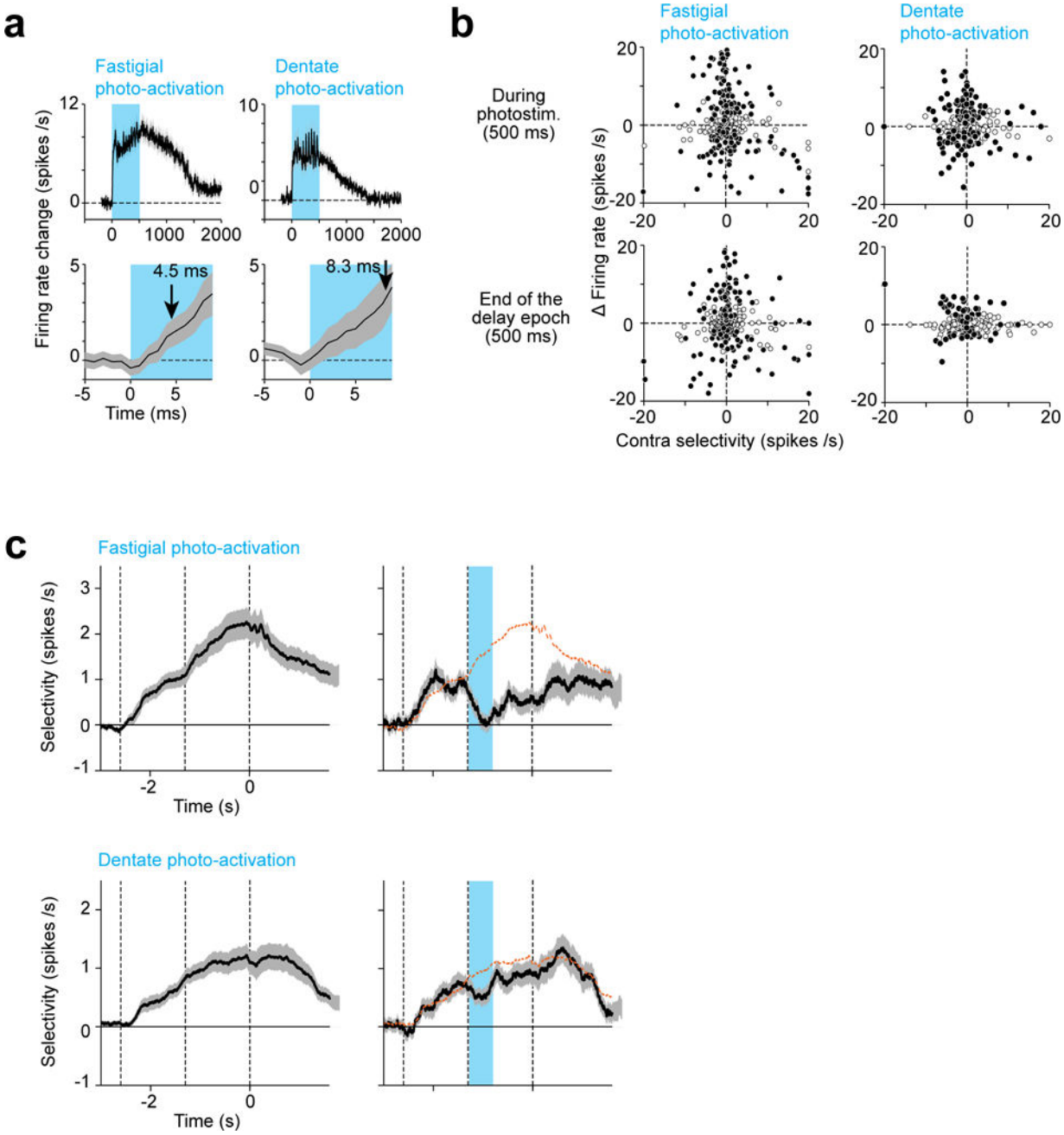

Extended Data Figure 9. CN ChR2 photo-activation drives rapid ALM activity change.

a. ALM neurons firing rate change during fastigial or dentate ChR2 photo-activation. Firing rate change is the difference in spike rate between control and photo-activation trials. For neurons that were suppressed by CN photo-activation, the firing rate differences are multiplied by −1 so that the firing rate changes are always positive for latency quantifications. Mean ± s.e.m. across neurons. Only neurons that were significantly modulated by CN photo-activation are included ($p<0.01$, two-tailed t-test; fastigial photo-activation, n=227; dentate photo-activation, n=163). *Top*, ALM firing rate change time course. Cyan, CN photo-activation (500ms). *Bottom*, ALM firing rate change onset (arrows). Firing rate change is quantified in 10ms time bins in 1ms steps. The onset time is the first time bin in which population firing rate change significantly deviated from 0 ($p<0.01$, two-tailed t-test). We repeated the onset time estimation 10,000 times. In each round, we re-sampled with replacement from the neurons in the dataset and re-estimated the onset time. The arrows indicate the mean estimated onset time.

b. Relationship between selectivity of individual ALM neurons and changes in firing rate due to CN photo-activation. Filled circles, ALM neurons that were significantly modulated by CN photo-activation ($p<0.01$, two-tailed t-test). Firing rate change is the difference in spike rate between control and photo-activation trials during photostimulation (*top*) or last 500ms of the delay epoch (*bottom*). Selectivity is the spike rate difference between “lick right” and “lick left” trials during the delay epoch.

c. ALM population selectivity from control and photo-activation trials (mean ± s.e.m. across neurons, bootstrap; selective neurons tested for >3 trials in all conditions). Orange dashed line, mean from control trials. *Top*, fastigial photo-activation (n=328); *bottom*, dentate photo-activation (n=377). Cyan, photo-activation.

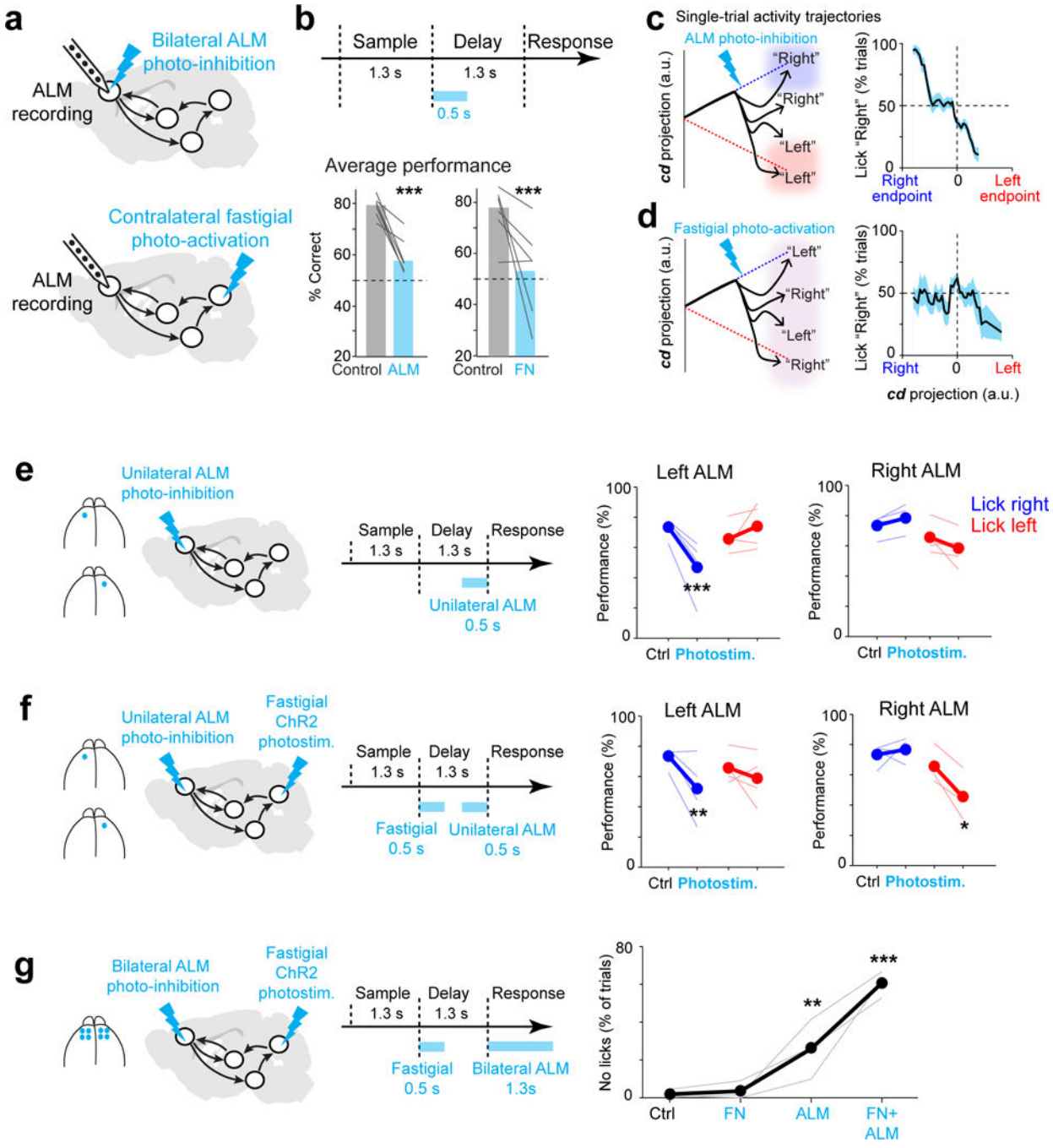

Extended Data Figure 10. Fastigial photo-activation destroys the relationship between ALM activity and upcoming movements

a. ALM recording during bilateral ALM photo-inhibition (*top*) or contralateral fastigial photo-activation (*bottom*).

b. Performance in control (grey) and photostimulation trials (cyan). "Lick left" and "lick right" trials are pooled. Chance is 50% (dashed line). Lines, individual mice (ALM photo-inhibition, n=7; fastigial photo-activation, n=6). ***, $p<0.001$, one-sided test, bootstrap (Methods).

c. *Left*, schematic. Dashed lines, control trials, ALM activity trajectories converge to discrete endpoints at the end of the delay epoch that predict upcoming movement directions ("lick right", blue; "lick left", red). Solid black lines, bilateral ALM photo-inhibition trials, the distance of the perturbed trajectories to the endpoints predicts future movement directions even though behavioral performance is near chance. *Right*, experimental data. Probability of the mouse licking right as a function of trajectory distance to the endpoints along the ***cd*** (Methods). Bilateral ALM photo-inhibition trials only (n=690). The ***cd*** and endpoints were estimated from independent control trials. Data are binned along the ***cd*** projection. s.e.m. is obtained by bootstrapping the trials in each bin.

d. Same as **c**, but for fastigial photo-activation trials (n=337). ALM activity no longer predicts future movement directions after a fastigial perturbation.

e. It is possible that fastigial perturbation activated downstream motor circuits that could maintain the motor plan and generate movements independent of ALM. We examined the necessity of ALM activity in driving directional licking after a fastigial perturbation. In VGAT-ChR2-EYFP mice expressing ChR2 in both Purkinje neurons and cortical GABAergic neurons, we independently manipulated activity in the fastigial nucleus and ALM (Methods). *Left*, unilateral ALM photo-inhibition during the late delay epoch. *Right*, behavioral performance for each trial type in control and photo-inhibition trials. Left ALM photo-inhibition biased upcoming licking to the left, resulting in lower performance in the "lick right" trials. The opposite pattern of bias was induced by right ALM photo-inhibition. Thick lines, mean; thin lines, individual mice (n=4). ***, p=0.0002, one-sided test, bootstrap (Methods).

f. Same as **e**, but for unilateral ALM photo-inhibition after fastigial perturbation. Note the same pattern of behavioral bias as **e**. *, p=0.04, **, p=0.008, one-sided test, bootstrap.

g. *Left*, after fastigial perturbation, ALM activity was bilaterally silenced during movement initiation. *Right*, fraction of trials in which mice did not lick after the 'go' cue. FN, fastigial perturbation only; ALM, bilateral ALM photo-inhibition; FN+ALM, fastigial perturbation followed by bilateral ALM photo-inhibition. Thick lines, mean; thin lines, individual mice (n=3). **, p=0.002, ***, p=0.0002, one-sided test, bootstrap.

Supplementary Material

Refer to Web version on PubMed Central for supplementary material.

Acknowledgements

We thank Roy Sillitoe for L7-cre mice, Javier Medina, Hidehiko Inagaki, Zengcai Guo, and Misha Ahrens for comments on the manuscript, Shaul Druckmann for discussion, Tina Pluntke, Miho Inagaki for animal training, Joshua White, Hana Hasanbegovic for dystonia scoring. This work was funded by the Robert and Janice McNair Foundation (N.L.), Whitehall Foundation (N.L.), Alfred P. Sloan Foundation (N.L.), Searle Scholars Program (N.L.), NIH NS104781 (N.L.), Simons Collaboration on the Global Brain (K.S., N.L.), the Dutch Organization for Medical Sciences (C.I.D.Z.), Life Sciences (Z.G., C.I.D.Z.), ErasmusMC fellowship (Z.G.), the ERC-advanced and ERC-PoC (C.I.D.Z.), and Howard Hughes Medical Institute (K.S., M.E., N.L.).

References

1. Tanji J & Evarts EV Anticipatory activity of motor cortex neurons in relation to direction of an intended movement. Journal of neurophysiology 39, 1062–1068 (1976). [PubMed: 824409]

2. Funahashi S, Bruce CJ & Goldman-Rakic PS Mnemonic coding of visual space in the monkey's dorsolateral prefrontal cortex. Journal of neurophysiology 61, 331–349 (1989). [PubMed: 2918358]
3. Riehle A & Requin J Monkey primary motor and premotor cortex: single-cell activity related to prior information about direction and extent of an intended movement. Journal of neurophysiology 61, 534–549 (1989). [PubMed: 2709098]
4. Fried I, Mukamel R & Kreiman G Internally generated preactivation of single neurons in human medial frontal cortex predicts volition. Neuron 69, 548–562, 10.1016/j.neuron.2010.11.045 (2011). [PubMed: 21315264]
5. Murakami M, Vicente MI, Costa GM & Mainen ZF Neural antecedents of self-initiated actions in secondary motor cortex. Nature neuroscience 17, 1574–1582 (2014). [PubMed: 25262496]
6. Svoboda K & Li N Neural mechanisms of movement planning: motor cortex and beyond. Current opinion in neurobiology In press (2017).
7. Goldman-Rakic PS Cellular basis of working memory. Neuron 14, 477–485 (1995). [PubMed: 7695894]
8. Wang XJ Synaptic reverberation underlying mnemonic persistent activity. Trends Neurosci 24, 455–463 (2001). [PubMed: 11476885]
9. Wolpert DM, Miall RC & Kawato M Internal models in the cerebellum. Trends Cogn Sci 2, 338–347 (1998). [PubMed: 21227230]
10. Proville RD et al. Cerebellum involvement in cortical sensorimotor circuits for the control of voluntary movements. Nature neuroscience 17, 1233–1239, 10.1038/nn.3773 (2014). [PubMed: 25064850]
11. Heiney SA, Kim J, Augustine GJ & Medina JF Precise control of movement kinematics by optogenetic inhibition of Purkinje cell activity. The Journal of neuroscience : the official journal of the Society for Neuroscience 34, 2321–2330, 10.1523/JNEUROSCI.4547-13.2014 (2014). [PubMed: 24501371]
12. Herzfeld DJ, Kojima Y, Soetedjo R & Shadmehr R Encoding of action by the Purkinje cells of the cerebellum. Nature 526, 439–442, 10.1038/nature15693 (2015). [PubMed: 26469054]
13. Schmahmann JD & Sherman JC The cerebellar cognitive affective syndrome. Brain : a journal of neurology 121 (Pt 4), 561–579 (1998). [PubMed: 9577385]
14. Ito M Control of mental activities by internal models in the cerebellum. Nature reviews. Neuroscience 9, 304–313, 10.1038/nrn2332 (2008). [PubMed: 18319727]
15. Strick PL, Dum RP & Fiez JA Cerebellum and nonmotor function. Annual review of neuroscience 32, 413–434, 10.1146/annurev.neuro.31.060407.125606 (2009).
16. Tsai PT et al. Autistic-like behaviour and cerebellar dysfunction in Purkinje cell Tsc1 mutant mice. Nature 488, 647–651, 10.1038/nature11310 (2012). [PubMed: 22763451]
17. Guo ZV et al. Maintenance of persistent activity in a frontal thalamocortical loop. Nature 545, 181–186, 10.1038/nature22324 (2017). [PubMed: 28467817]
18. Wagner MJ, Kim TH, Savall J, Schnitzer MJ & Luo L Cerebellar granule cells encode the expectation of reward. Nature 544, 96–100, 10.1038/nature21726 (2017). [PubMed: 28321129]
19. Guo ZV et al. Flow of cortical activity underlying a tactile decision in mice. Neuron 81, 179–194 (2014). [PubMed: 24361077]
20. Li N, Daie K, Svoboda K & Druckmann S Robust neuronal dynamics in premotor cortex during motor planning. Nature, 10.1038/nature17643 (2016).
21. Chen TW, Li N, Daie K & Svoboda K A Map of Anticipatory Activity in Mouse Motor Cortex. Neuron 94, 866–879 e864, 10.1016/j.neuron.2017.05.005 (2017). [PubMed: 28521137]
22. Inagaki HK, Inagaki M, Romani S & Svoboda K Low-Dimensional and Monotonic Preparatory Activity in Mouse Anterior Lateral Motor Cortex. The Journal of neuroscience : the official journal of the Society for Neuroscience 38, 4163–4185, 10.1523/JNEUROSCI.3152-17.2018 (2018). [PubMed: 29593054]
23. Li N, Chen TW, Guo ZV, Gerfen CR & Svoboda K A motor cortex circuit for motor planning and movement. Nature 519, 51–56 (2015). [PubMed: 25731172]
24. Economo MN et al. Distinct descending motor cortex pathways 1 and their roles in movement. bioRxiv, 10.1101/229260. (2017).

25. McElvain LE et al. Circuits in the rodent brainstem that control whisking in concert with other orofacial motor actions. Neuroscience 368, 152–170, 10.1016/j.neuroscience.2017.08.034 (2018). [PubMed: 28843993]
26. Medina JF & Mauk MD Computer simulation of cerebellar information processing. Nature neuroscience 3 Suppl, 1205–1211, 10.1038/81486 (2000). [PubMed: 11127839]
27. Ohyama T, Nores WL, Murphy M & Mauk MD What the cerebellum computes. Trends Neurosci 26, 222–227, 10.1016/S0166-2236(03)00054-7 (2003). [PubMed: 12689774]
28. Kalmbach BE, Ohyama T, Kreider JC, Riusech F & Mauk MD Interactions between prefrontal cortex and cerebellum revealed by trace eyelid conditioning. Learn Mem 16, 86–95, 10.1101/lm.1178309 (2009). [PubMed: 19144967]
29. Shenoy KV, Sahani M & Churchland MM Cortical control of arm movements: a dynamical systems perspective. Annual review of neuroscience 36, 337–359, 10.1146/annurev-neuro-062111-150509 (2013).
30. Inagaki HK, Fontolan L, Romani S & Svoboda K Discrete attractor dynamics underlying selective persistent activity in frontal cortex. bioRxiv, 10.1101/203448 (2017).
31. Lewis PM, Gritli-Linde A, Smeyne R, Kottmann A & McMahon AP Sonic hedgehog signaling is required for expansion of granule neuron precursors and patterning of the mouse cerebellum. Dev Biol 270, 393–410, 10.1016/j.ydbio.2004.03.007 (2004). [PubMed: 15183722]
32. Madisen L et al. A toolbox of Cre-dependent optogenetic transgenic mice for light-induced activation and silencing. Nature neuroscience 15, 793–802 (2012). [PubMed: 22446880]
33. Zhao S et al. Cell type-specific channelrhodopsin-2 transgenic mice for optogenetic dissection of neural circuitry function. Nature methods 8, 745–752 (2011). [PubMed: 21985008]
34. Guo ZV et al. Procedures for behavioral experiments in head-fixed mice. PloS one 9, e88678 (2014). [PubMed: 24520413]
35. Chen CH, Fremont R, Arteaga-Bracho EE & Khodakhah K Short latency cerebellar modulation of the basal ganglia. Nature neuroscience 17, 1767–1775, 10.1038/nn.3868 (2014). [PubMed: 25402853]
36. Rossi MA et al. A GABAergic nigrotectal pathway for coordination of drinking behavior. Nature neuroscience 19, 742–748, 10.1038/nn.4285 (2016). [PubMed: 27043290]
37. Dong HW The Allen reference atlas: A digital color brain atlas of the C57Bl/6J male mouse (John Wiley & Sons Inc, 2008).
38. Oh SW et al. A mesoscale connectome of the mouse brain. Nature 508, 207–214 (2014). [PubMed: 24695228]
39. Rueckert D et al. Nonrigid registration using free-form deformations: application to breast MR images. IEEE Trans Med Imaging 18, 712–721, 10.1109/42.796284 (1999). [PubMed: 10534053]

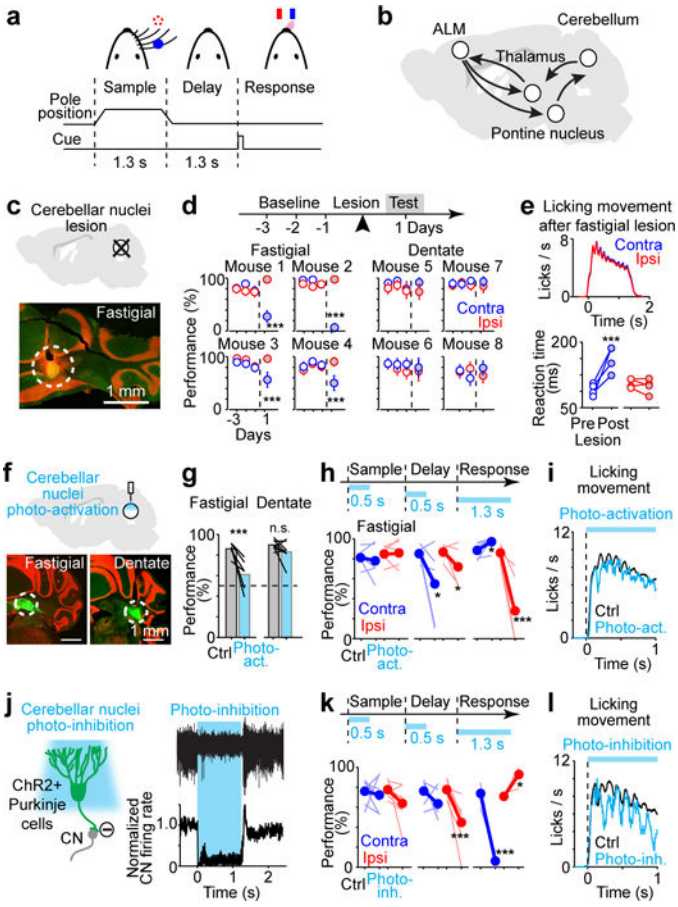

Figure 1. Cerebellar involvement in motor planning and movement initiation.

a. Mouse reporting the location of a pole by directional licking.

b. ALM-cerebellar loop.

c. Fastigial or dentate lesion. *Bottom*, example lesion.

d. Behavioral performance (session mean ± s.e.m., n=75–256 trials). Mouse 1–2, left fastigial lesion; mouse 3–4, right fastigial; mouse 5, left dentate; mouse 6–8, right dentate. “Lick left” and “lick right” trials are grouped by instructed licking direction relative to the lesioned hemisphere. Blue, contralesional; red, ipsilesional. ***, p<0.001, one-sided test, pre- versus post lesion, bootstrap (Methods).

e. *Top*, lick rate during contra- and ipsilesional licking bouts after fastigial lesion. Lick times are aligned to the first lick (t=0). *Bottom*, time of the first lick to the contra- and ipsilesional direction after the ‘go’ cue onset. Lines, individual mice (n=4). ***, p<0.001, one-sided test, bootstrap.

f. Fastigial or dentate photo-activation. Laser power, 0.5–1.5 mW. *Bottom*, example ChR2 expression.

g. Fastigial or dentate photo-activation during the delay epoch. Behavioral performance. “Lick left” and “lick right” trials are pooled. Chance is 50% (dashed line). Lines, individual mice (fastigial, n=6; dentate, n=8). Bars, mean. ***, p<0.001, one-sided test, bootstrap.

h. Fastigial photo-activation during specific epochs. Behavioral performance for each trial type. “Lick left” and “lick right” trials are grouped by instructed licking direction relative to

the manipulated hemisphere. Blue, contralateral; red, ipsilateral. Both hemispheres were tested. See Supplemental Table 1 for manipulated hemispheres. Thick lines, mean; thin lines, individual mice (n=6). *, p<0.05, ***, p<0.001, one-sided test, bootstrap.

i. Lick rate in control and fastigial photo-activation trials (n=6 mice).

j. *Left*, schematic of CN photo-inhibition. Laser power, 0.5–4.5 mW. *Right*, silicon probe recording in the fastigial nucleus. Example voltage trace and average firing rate (n=26 neurons, 2 mice). Firing rates were normalized to baseline (500ms before photostimulus onset).

k. CN photo-inhibition. Same as

h. n = 7 mice for sample and delay epoch photo-inhibition; n=3 for response epoch photo-inhibition (Supplemental Table 1).

l. Lick rate in control and CN photo-inhibition trials (n = 3 mice).

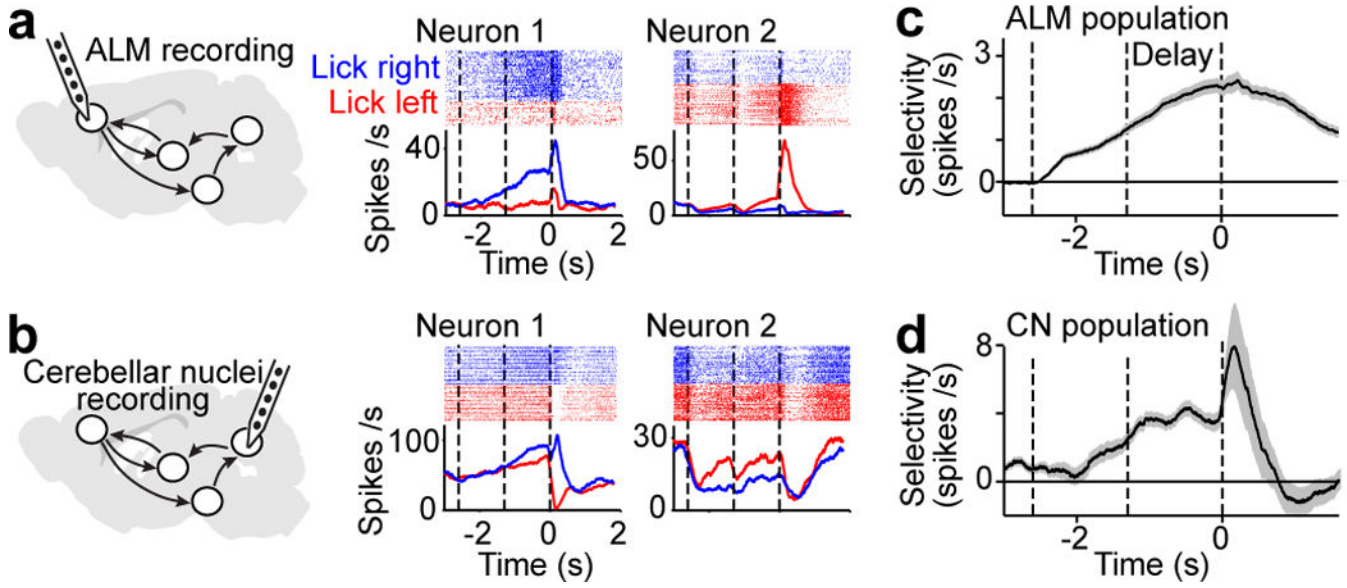

Figure 2. Preparatory activity in ALM and CN

a. Silicon probe recording in ALM. 2 example neurons. *Top*, spike raster. *Bottom*, spike rate. Correct “lick right” (blue) and “lick left” (red) trials only. Dashed lines, behavioral epochs.

b. Same as **a**, but for CN.

c. ALM population selectivity (mean ± s.e.m. across neurons, bootstrap). Selectivity is the spike rate difference between the preferred and non-preferred trial type (Methods). Putative pyramidal neurons with significant selectivity (n=980). Averaging window, 200 ms.

d. Same as **c**, but for CN. Neurons with significant selectivity (n=197).

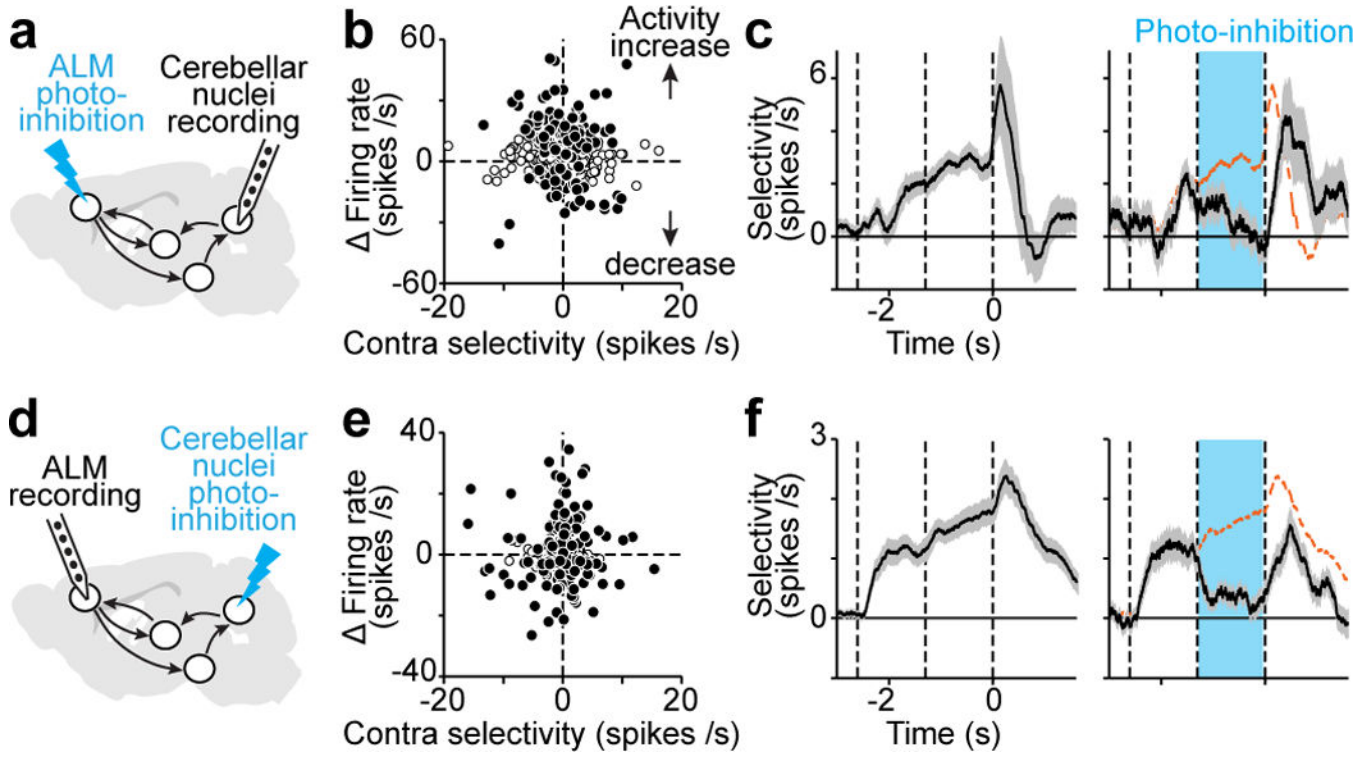

Figure 3. CN preparatory activity depends on ALM activity and *vice versa*

a. CN recording during bilateral ALM photo-inhibition. Laser power, 1.5 mW per location (Methods).

b. Relationship between delay epoch selectivity of individual CN neurons and changes in firing rate due to ALM photo-inhibition (n=389). Filled circles, neurons significantly modulated by ALM photo-inhibition ($p<0.01$, two-tailed t-test).

c. CN population selectivity. *Left*, control; *right*, photo-inhibition trials. Mean ± s.e.m. across neurons, bootstrap. Selective neurons tested for >3 trials in all conditions (n=157). Orange line, mean from control trials.

d. ALM recording during contralateral CN photo-inhibition. Laser power, 1.5–4.5 mW.

e. Same as **b**, but for ALM neurons (n=454).

f. Same as **c**, but for ALM neurons (n=329).

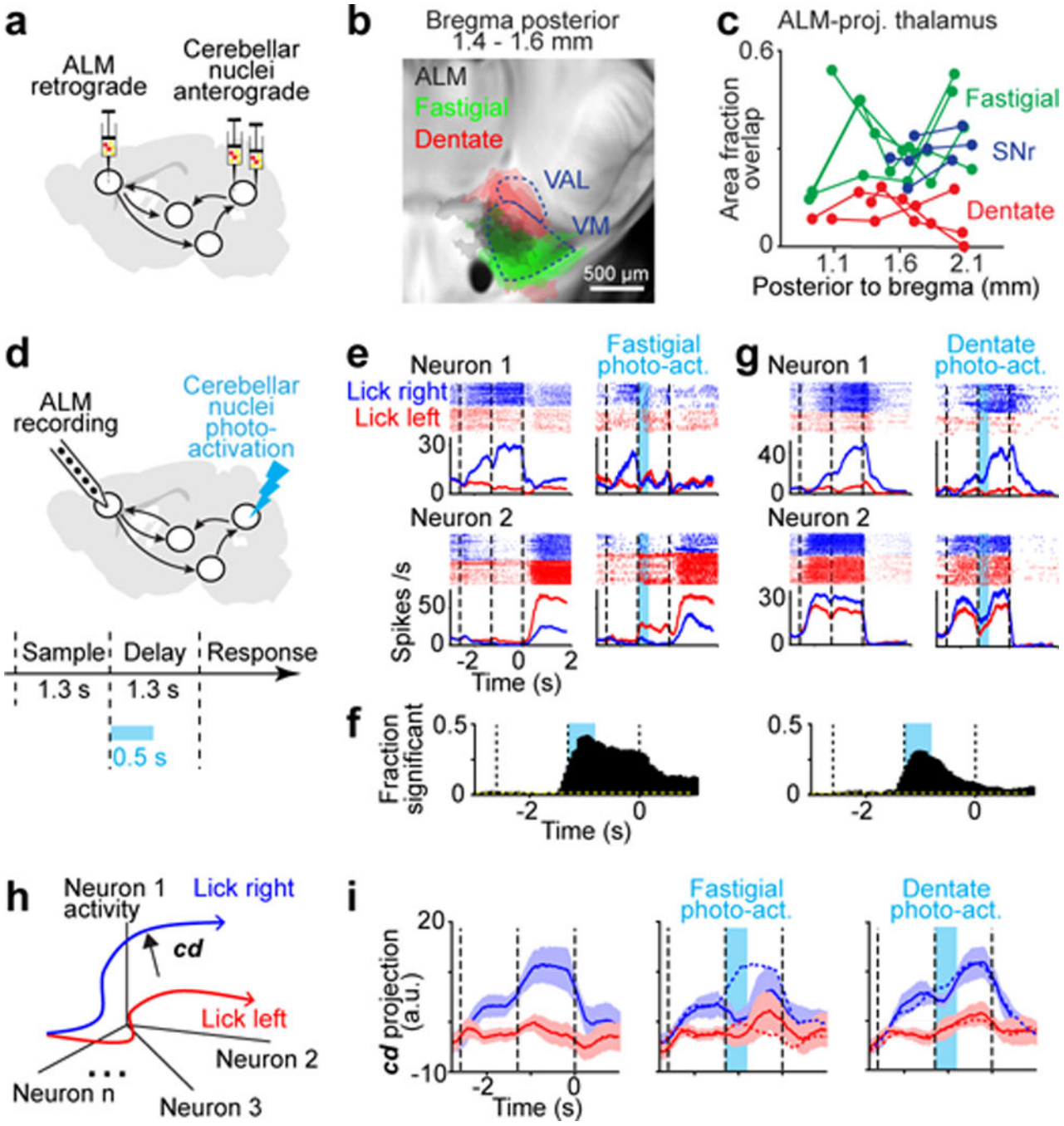

Figure 4. Fastigial nucleus is critical for ALM coding of future movement

a. Triple injections to map connectivity in the thalamus.

b. *Left*, labeled areas in the thalamus from fastigial (green, n=6), dentate (red, n=4), and ALM (black, n=8) injections. Brain sections were aligned to the Allen Reference Brain (Methods). VM and VAL borders are based on the Allen Reference Atlas. Labeling were also present in the medial dorsal thalamus but are not quantified here.

c. Overlaps between ALM-projecting thalamus and projections from the fastigial nucleus, dentate nucleus, or basal ganglia substantia nigra reticulata (SNr). The co-labeled area is

normalized to the total thalamic area labeled by each projection ('area fraction overlap'). Dots, individual coronal sections. Lines, individual injections.

d. ALM recording during contralateral fastigial or dentate photo-activation. Laser power, 0.5–1.5 mW.

e. Example ALM neurons.

f. Fraction of neurons with significant spike rate change compared to control trials ($p<0.01$, two-tailed t-test). n=446. Cyan, photo-activation.

g. Same as **e** and **f**, but for dentate photo-activation. n=466.

h. Schematic, movement-specific activity trajectories and coding direction (***cd***) in activity space.

i. ALM activity in control and photo-activation trials projected onto the ***cd***. Both correct and error trials, grouped by instructed movement. Mean ± s.e.m (28 sessions, 10 mice). The ***cd*** was estimated using an independent subset of control trials (correct trials only).